

Article

Transtension at the Northern Termination of the Alfeo–Etna Fault System (Western Ionian Sea, Italy): Seismotectonic Implications and Relation with Mt. Etna Volcanism

Salvatore Gambino ¹, Giovanni Barreca ^{1,2}, Valentina Bruno ³, Giorgio De Guidi ^{1,2}, Carmelo Ferlito ^{1,3}, Felix Gross ^{4,5}, Mario Mattia ³, Luciano Scarfi ³ and Carmelo Monaco ^{1,2,3,*}

¹ Dipartimento di Scienze Biologiche Geologiche e Ambientali, Università di Catania, 95129 Catania, Italy; salvatore.gambino@unict.it (S.G.); giovanni.barreca@unict.it (G.B.); giorgio.deguidi@unict.it (G.D.G.); carmelo.ferlito@unict.it (C.F.)

² CRUST—Interuniversity Center for 3D Seismotectonics with Territorial Applications, 66100 Chieti, Italy

³ Istituto Nazionale di Geofisica e Vulcanologia, Osservatorio Etneo—Sezione di Catania, 95125 Catania, Italy; valentina.bruno@ingv.it (V.B.); mario.mattia@ingv.it (M.M.); luciano.scarfi@ingv.it (L.S.)

⁴ Institute of Geosciences, Kiel University, 24148 Kiel, Germany; felix.gross@ifg.uni-kiel.de

⁵ Center for Ocean and Society, Kiel University, 24148 Kiel, Germany

* Correspondence: cmonaco@unict.it; Tel.: +39-095-7195731

Citation: Gambino, S.; Barreca, G.; Bruno, V.; De Guidi, G.; Ferlito, C.; Gross, F.; Mattia, M.; Scarfi, L.; Monaco, C. Transtension at the Northern Termination of the Alfeo–Etna Fault System (Western Ionian Sea, Italy): Seismotectonic Implications and Relation with Mt. Etna Volcanism. *Geosciences* **2022**, *12*, 128. <https://doi.org/10.3390/geosciences12030128>

Academic Editors: Jesus Martinez-Frias and Olivier Lacombe

Received: 14 January 2022

Accepted: 7 March 2022

Published: 10 March 2022

Publisher's Note: MDPI stays neutral with regard to jurisdictional claims in published maps and institutional affiliations.



Copyright: © 2022 by the authors. Licensee MDPI, Basel, Switzerland. This article is an open access article distributed under the terms and conditions of the Creative Commons Attribution (CC BY) license (<http://creativecommons.org/licenses/by/4.0/>).

Abstract: Offshore data in the western Ionian Sea indicate that the NW–SE-trending dextral shear zone of the Alfeo–Etna Fault System turns to the N–S direction near the Ionian coastline, where the extensional Timpe Fault System is located. Morpho-structural data show that NW–SE-trending right-lateral strike-slip faults connect the Timpe Fault System with the upper slope of the volcano, where the eruptive activity mainly occurs along the N–S to NE–SW-trending fissures. Fault systems are related to the ~E–W-trending extension and they are seismically active having given rise to shallow and low-moderate magnitude earthquakes in the last 150 years. As a whole, morpho-structural, geodetic and seismological data, seismic profiles and bathymetric maps suggest that similar geometric and kinematic features characterize the shear zone both on the eastern flank of the volcano and in the Ionian offshore. The Alfeo–Etna Fault System probably represents a major kinematic boundary in the western Ionian Sea associated with the Africa–Europe plate convergence since it accommodates, by right-lateral kinematics, the differential motion of adjacent western Ionian compartments. Along this major tectonic alignment, crustal structures such as releasing bends, pull-apart basins and extensional horsetails occur both offshore and on-land, where they probably represent the pathway for magma uprising from depth.

Keywords: Ionian Sea; Mt. Etna; seismic reflection data; GNSS data; tectonic-driven volcanism

1. Introduction

The Mt. Etna volcanic edifice sits atop the collisional belt formed because of the convergence between African and European plates, at the footwall of large transtensional faults along the eastern coast of Sicily (Figure 1 [1,2]). At the Mt. Etna volcano, eruptions occur most frequently in the summit area; here the magma is driven to the surface through the central axis, which is in turn associated to the extensional tectonics that have their highest expression right in the summit craters [3–5]. However, the volcano is also characterized by lateral eruptions occurring on its flanks [6]. The origin of such lateral eruptions is not always clear. In some examples, the geometric association of the eruptive fissures with the central axis is evident, but in many other cases the correlation is missing and volcanism could have a predominantly tectonic origin (e.g., [7]). This is particularly true for eruptions in the south-eastern sector of the volcanic edifice, where large monogenetic pyroclastic cones are aligned with tectonic structures.

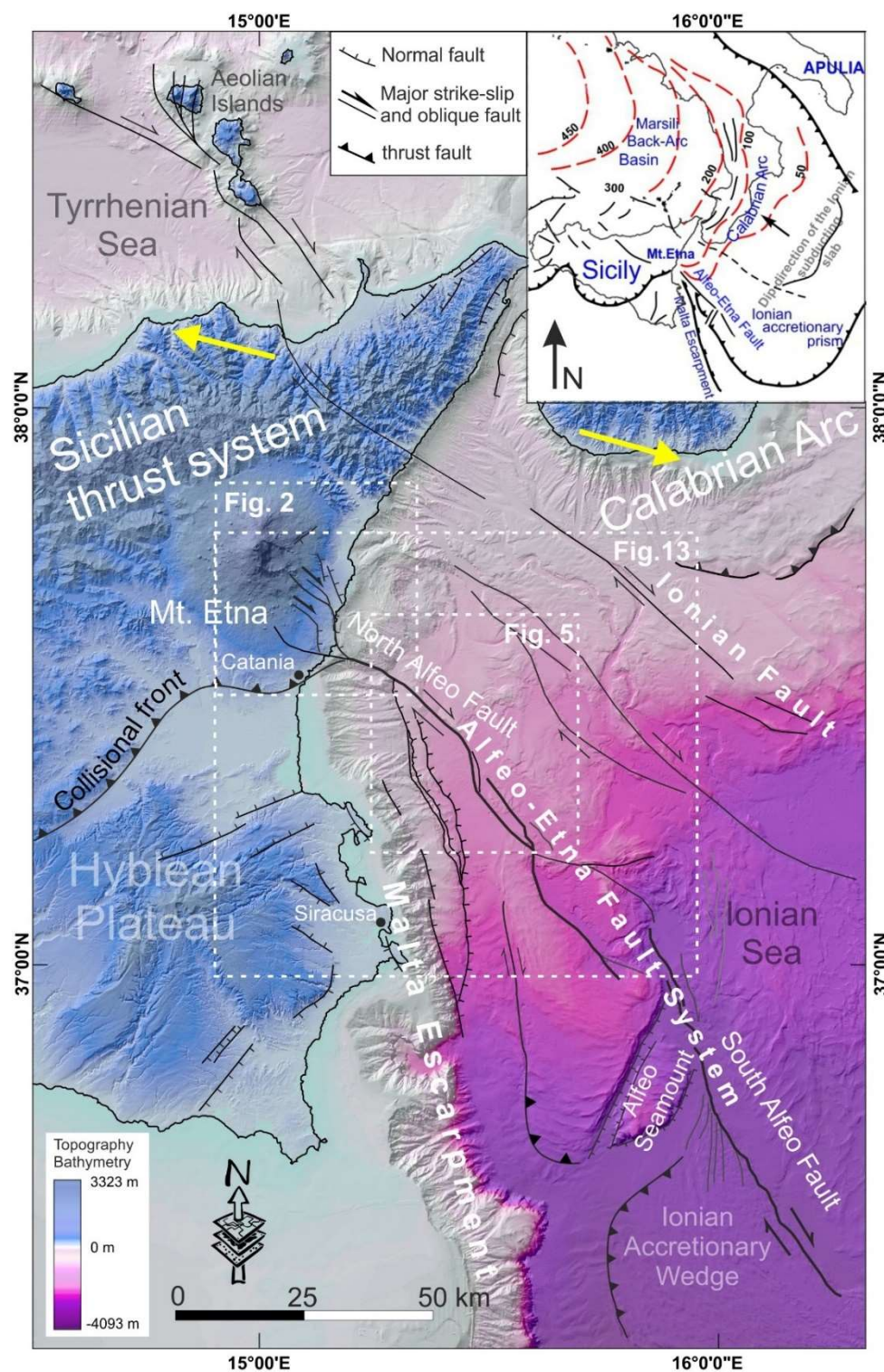


Figure 1. Tectonic sketch-map of eastern Sicily and the Ionian offshore (from [8] modified). The main tectonic features are from Polonia et al. [9] and Gutscher et al. [10]. Yellow arrows indicate the direction of geodetic extension between Sicily and the Calabria–Ionian sector (from Palano et al. [11]; De Guidi et al. [12]; D’Agostino and Selvaggi [13]; Serpelloni et al. [14]). Inset shows the location of Mt. Etna in the geodynamic framework of the eastern Mediterranean, at the southern edge of the subducting Ionian slab (dashed lines with numbers indicate its depth in km).

The geodynamic of the eastern flank of the volcano is characterized by normal faulting along a tectonic belt affecting the coastal sector, named the “Timpe Fault System” [15], and by right-transtensive motion along several associated structures upstream [3,16–

22]. The tectonic activity of the eastern flank of Mt. Etna must be framed within the geodynamic context of north-eastern Sicily and the western Ionian Sea, where regional processes occur [11,13,14,23–29]. In particular, according to Monaco et al. [30], the Timpe Fault System connects the transtensional faults characterizing the south-eastern sector of the volcano with a regional shear zone that extends offshore (the Alfeo–Etna Fault System of Polonia et al. [9]; the North Alfeo Fault System of Gutscher et al. [10]; Figure 1).

This study, based on an interdisciplinary approach that includes field observations, an analysis of seafloor bathymetry and seismic reflection profiles and seismological and geodetic data, allows the kinematic relation between the structures occurring in the south-eastern flank of Mt. Etna (including the Timpe Fault System) and the shear zone extending to the offshore in the Ionian Sea (Figure 1) to be defined. In addition, possible implications with volcanic activity are examined. The interpretation makes use of numerous studies already published by our research group (e.g., [2–5,9–11,18,22,28,30]), integrated by new seismological and marine geology data recently acquired in the offshore.

2. Geological Setting

2.1. Mt. Etna Volcano

The Mt. Etna volcano was formed along a diverging belt in the framework of the Africa–Europe plate convergence. In particular, it lies on the Ionian coast of Sicily, between the collisional front of the Sicilian thrust system to the north and the flexured margin of the Hyblean foreland to the south (Figure 1). Its origin has been related to the melting of asthenospheric material due to decompression at the south-western border of the roll-backed Ionian slab subducting beneath the Tyrrhenian lithosphere [23–25,28]. Since the Middle Pleistocene, contractional structures related to the approximately NNW–SSE compressive regional tectonic regime at the collisional front [31,32] have been coupled with oblique transtensional faults across the western Ionian Basin. These faults form a lithospheric boundary characterized by strong seismicity and active volcanism, which extends from the Aeolian Islands, at the south-western edge of the Ionian subduction system [12,33,34], to the offshore of eastern Sicily, including the NW–SE-trending Ionian fault and Alfeo–Etna fault systems (Figure 1; [9] and reference therein).

The structural framework of the Mt. Etna volcano, as well as the flank instability and the intrusion of feeding dikes, is the result of an interaction between regional tectonics and magmatic processes operating at the local scale [3,7,35,36]. Crustal stretching and associated fracturing favoured magma ascent in the last 500 ka [1–3]. In particular, between 220 and 120 ka, volcanism in the Mt. Etna region concentrated on N–S-trending eruptive fissures located along the Ionian coast, corresponding to the Timpe Fault System (the Timpe phase, [1,6,37]). In that period, the transtension favoured the ascent of alkaline magma, transforming the previous scattered fissural volcanism into central volcanic activity that shifted westward to build the present edifice from 100 ka ago to the present day [1,2].

The eastern lower slope of Mt. Etna, crossed by the extensional NNW–SSE to N–S-trending Timpe Fault System and by NW–SE-oriented strike-slip and oblique structures (Figure 2), is the most tectonically active area of the volcanic edifice both for the number of volcano-tectonic seismic events and for the maximum intensity reached at the epicentre [38]. Unlike the western sector of the volcano, where seismicity also occurs at greater depths (down to 35 km) related to the regional NNW–SSE-oriented compression [28,39,40], on the eastern sector the intense tectonic activity of the Timpe Fault System is characterized by several shallow earthquakes (more than 80% being shallower than 5 km) with a medium-low magnitude (magnitude seldom exceeding 4; [38,41,42]). In general, being very shallow, they cause significant damage relative to the magnitude (epicentral macroseismic intensity up to IX), even though in very narrow areas, they are often accompanied by coseismic surface fracturing [8,10,42]. In the south-eastern sector of the volcano, the NW–SE-trending Fiandaca, Linera-Santa Tecla and Santa Venerina faults [32] connect by right-lateral motion the Timpe Fault System with the upper slope of the

volcano, where the recent eruptive activity has concentrated along the southern and north-eastern rift zones [2–4,6,11]. It is worth noting that fault reactivation can be triggered by the sudden upraise of feeding dikes [43–46].

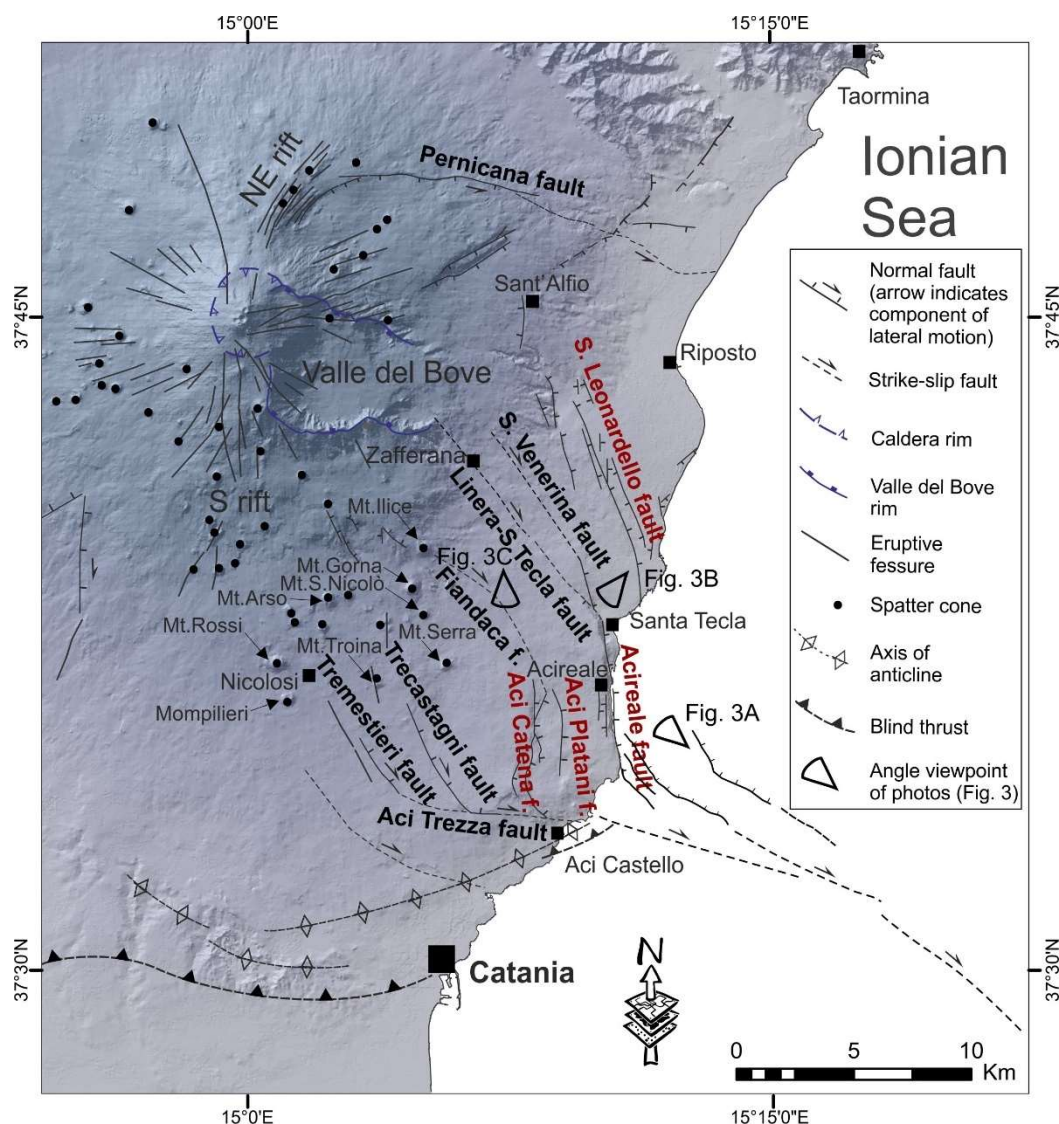


Figure 2. Structural map of Mt. Etna (from [18,22,47] modified; see location in Figure 1). Faults labelled in a red colour belong to the Timpe Fault System. The eastern sector of the Pernicana Fault and the Aci Trezza Fault aseismically transfer the extension towards the offshore and limit to the north and to the south, respectively, the sliding sector of the volcanic edifice (see [36]).

The geometry and the sense of movement of most of the main active structures present on the eastern flank of the volcano (Figure 2), both the seismogenic faults (normal, strike-slip or oblique) and eruptive fractures (often marked by aligned spatter cones) are kinematically consistent, since they accommodate at a crustal depth regional NNW–SSE-oriented compression and an ~E–W-oriented extension [3,39,40,48–50]. In the sedimentary basement of the volcano, the NNW–SSE-oriented regional compression has been accommodated by the deep thrusting and detachment folding of Pleistocene foredeep and coastal–alluvial deposits along the southern margin of the volcanic edifice [31,51,52]. GPS measurements over the last 20 years have revealed a shortening rate of ~5 mm/yr along a NNW–SSE-oriented axis of compression, consistent with the focal mechanism of deep earthquakes generated by the collisional front [32].

Structural, morphological and geophysical studies suggest that the eastern flank is also spreading seaward gravitationally through the slow motion of several mobile

shallow blocks mostly bounded by tectonic structures (see [36] for a review). The sliding sector (Figure 2) is confined to the west by the NE and S Rift zones passing through the summit craters, and to the north and to the south by the left-lateral Pernicana fault and by the right-lateral Aci Trezza faults, respectively [53], that aseismically transfer the extension to the east, towards the offshore [54]. The rate of the gravitational deformation is one order greater than the tectonic component [35], which, for this reason, could be masked. Nevertheless, uplifted paleo-shorelines at the footwall of normal faults, documented at the SE sector of the volcano [55], suggest that, in the long-term, the tectonic signal prevails over the gravitational signal.

2.2. Alfeo–Etna Fault System

The Alfeo–Etna Fault System [9] offshore Eastern Sicily, is a roughly 140 km long, NW–SE-trending, active, dextral strike-slip fault system running from the coastal segments of the Timpe Faults System to the Alfeo seamount (Figure 1). The occurrence of the Alfeo–Etna Fault System in the Mt. Etna offshore has been revealed by swath-bathymetry and multichannel seismic data (the North Alfeo Fault System of Gutscher et al. [10] and the Alfeo Fault System of Maesano et al. [27]).

According to Gutscher et al. [10], it is a Subduction-Transform Edge Propagator fault system (STEP sensu Govers and Wortel, [56]), consisting of northern and southern branches known as the North Alfeo Fault (about 60 km long) and the South Alfeo Fault (about 80 km long), respectively. Approaching the coastline of eastern Sicily, southeast of Mt. Etna, this fault system intersects the reactivated portion of the Malta Escarpment [57]. Bathymetric and seismic profiles suggest that the latter is crosscut by the Alfeo–Etna Fault System. The dextral strike-slip nature of the North Alfeo Fault has been inferred from earthquake focal mechanisms (Figure 1; [58]) and morpho-bathymetric expression [10], as well as from direct submarine scuba-diving observation of the displaced basaltic flow [59].

According to Polonia et al. [9], the Alfeo–Etna Fault System could also be associated with the relative motion of Africa and Eurasia since it accommodates, by dextral transtensional kinematics, the differential motion of adjacent western Ionian compartments (see also [11,29]). Seismic profiles and bathymetric maps [47,59] coherently indicate that the NW–SE-trending Alfeo–Etna Fault System turns to the N–S direction near the Ionian coastline (Figure 1) and it connects with the Timpe Fault System on-land, forming, as a whole, a releasing bend zone [30,47].

3. Tectonic Structures of the South-Eastern Sector of Mt. Etna

In this section, we summarize the data collected in the field and/or already published by our research group that are integrated with seismological and field data published by other authors (see references) and frame them in the geodynamic setting of the Alfeo–Etna shear zone.

The Timpe Fault System (Figure 2) controls the present topography and drainage network of the lower south-eastern flank of Mt. Etna and shows steep escarpments (locally named “Timpe”) with very young, mostly Late Pleistocene to Holocene, morphology. The most impressive scarps, up to 200 m high, extend discontinuously for about 20 km from Sant’Alfio to Acireale, where they affect sedimentary and volcanic rocks ranging in age from Early Pleistocene to historical times [6,18,60]. Minor structures are the San Leonardello, Aci Catena and Aci Platani faults (Figure 2).

The 7 km long Acireale fault (Figure 2) forms a N170E-oriented rectilinear scarp, up to 200 m high, whose southern portion runs along the coast forming a coastal cliff gradually decreasing southwards (Figure 3A). It offsets a volcanic sequence mostly made of the 200 to 100 ka-old volcanics, locally covered by historical lava flows. Its activity has been characterized by vertical slip-rates up to ~4 mm/yr in the last 35 ka [21]. Fossil organisms sampled from raised Holocene paleo-shorelines along the coastline indicate a short-term uplift-rate of 3 mm/yr [55]. Despite the high rates of vertical deformation recorded in the Holocene (see above), the Acireale fault did not give rise to coseismic fracturing in

historical times, having been characterized only by low intensity earthquakes ($I = V$; [19] and references therein) at the end of the 19th century.

North-west of Santa Tecla, the Acireale fault bends to the N140E direction and branches into two distinct segments characterized by a progressively minor vertical offset and poor morphologic evidence, being largely covered by historical and prehistoric lava flows [6,60]: the Linera–Santa Tecla and the Santa Venerina faults (Figure 2). The Linera–Santa Tecla fault extends in the N140E direction upslope, crossing the village of Zafferana and reaching the Valle del Bove area [21]. A polished fault surface on the volcanoclastic products is well exposed west of Santa Tecla (Figure 2); here, oblique slickenlines and Riedel fractures indicate a prevalent right-lateral component of slip (Figure 3B; see also [3]). This structure has often been reactivated during the last two centuries with an oblique-dextral component, highlighted by centimetric ground fracturing (e.g., the 1914 and 1952 seismic events; $I = VII - IX$; [19] and references therein). The Santa Venerina fault bends upslope in a N140E direction as well; it was reactivated with a dextral-oblique motion for a length of 5 km during the 29 October 2002 seismic event ($M = 4.4$), as shown by centimetric ground fracturing and the focal mechanism [7]. Similar macroseismic effects were reported during the 26 May 1879 ($I = VIII$; $M = 4.1$; [19] and references therein) and the February 1986 ($I = V - VII$; $M = 3$; [15]) earthquakes.

To the south, the ~5 km long and ~NW–SE-striking Fiandaca fault [19] is also characterized by poor morphologic evidence and oblique-dextral motion, as shown by ground ruptures and building damages detected during seismic events in the last two centuries. In particular, the 1894 ($I = VII - VIII$) and the 25 October 1984 ($I = VIII$; $M = 4.1$) earthquakes were accompanied by the development of dm-long NNW–SSE-oriented oblique-dextral fractures and N–S-oriented en-echelon extensional fractures ([19] and reference therein). Similar open ground fractures (Figure 3C), compatible with a NW–SE- oriented dextral shear zone, were formed during the 26 December 2018 earthquake ($M_w = 4.9$); this event has provided new insights for improving the knowledge of the kinematics of the Fiandaca fault and of the volcano-tectonic behaviour of the south-eastern flank of Mt. Etna [30,45,46,61]. Morpho-structural and seismological data indicate a dextral strike-slip movement on a sub-vertical NNW–SSE to WNW–ESE-oriented plane with the maximum surficial rupture involving terminal extension fractures at its southern end for a total length of about 8 km [62].

The Aci Catena and Aci Platani faults link to the southern end of the Fiandaca fault as a system of east-dipping normal faults in a direction between NNW–SSE and N–S (Figure 2). They displace 100–200 ka-old volcanics forming up to 100 m high cumulative scarps, partially covered by historical and prehistoric lava flows [6–60]. The analysis of historical documents indicates that since the second half of the 19th century these structures have mostly been the site of aseismic creep events that damaged buildings and roads at the bottom of the main fault scarps and along minor structures [63]. These aseismic creep episodes, characterized by centimetric open fractures, were coeval or immediately subsequent to seismic crises along the Fiandaca fault (e.g., the 1984 and 2018 events, [30,63]).

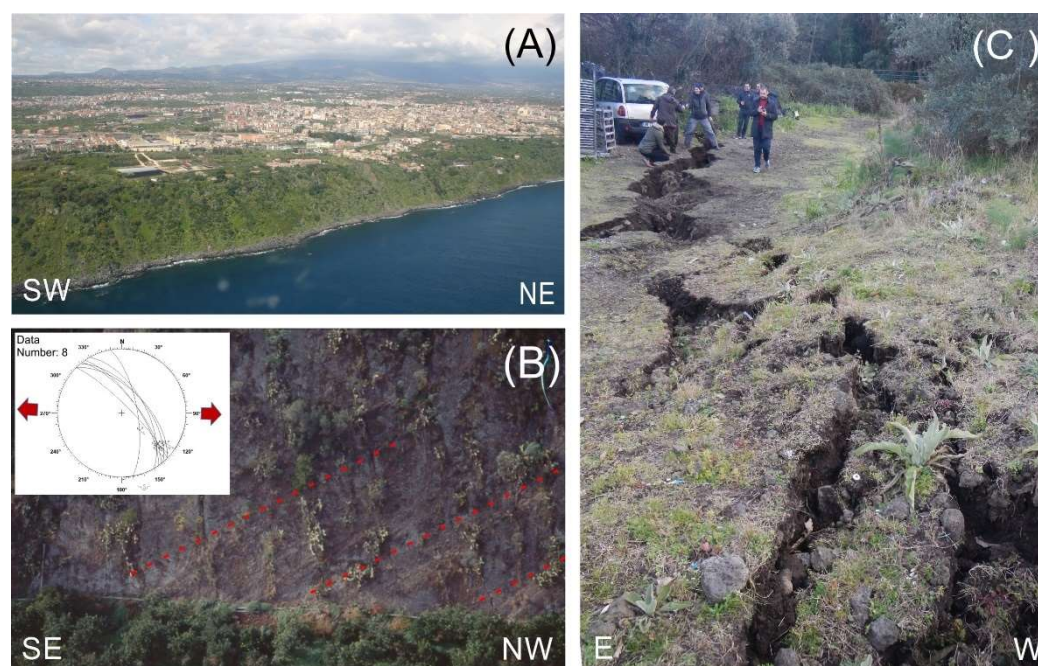


Figure 3. (A) View from the south-east of the Acireale Fault scarp. (B) View from the north-east of kinematic indicators of oblique motion (dextral-normal) along the south-eastern sector of the Linera–S.Tecla fault scarp; inset shows the stereographic projection (Daisy3 software) of fault planes and slickenlines measured in this site; the red arrows indicate the computed extension direction. (C) View from the north of the N–S-trending left-stepping en-echelon open ground fractures formed during the 26 December 2018 seismic event along the Fiandaca fault. See Figure 2 for locations.

West of the Aci Catena fault, two minor NW–SE-striking oblique faults often occur: the Trecastagni and the Tremestieri faults (Figure 2). They form 5 km and 3 km long scarps, respectively, up to 10 m high, covered by pre-historical and historical flows that in turn are offset by recent coseismic and creep movements. In particular, these structures have been reactivated (with oblique-dextral motion highlighted by centimetric ground fracturing on buildings, road walls and asphalt) during the 1980, 1988, 2005 and 2012 seismic events ($I = V - VII$; $M = 3.0-3.6$; [12,63,64]). The northern termination of these faults is characterized by alignments of monogenetic pyroclastic cones that reach large dimensions especially in the Trecastagni area (e.g., Mt. Arso, Mt. Gorna, Mt. Ilice, Mt. Serra, Mt. S. Nicolò, Mt. Troina; Figure 2). It is worth noting that the Tremestieri fault extends to the north-west, as far as Nicolosi, without morphological evidence (the hidden fault of Azzaro [13]), probably joining to the southern rift zones, which are also marked by large (e.g., Mompilieri, Mt. Rossi; Figure 2) and minor aligned spatter cones [3]. Extension along the Trecastagni and the Tremestieri faults is accommodated by a W–E-oriented and 7 km long fracture zone, the Aci Trezza fault [11,65], without topographic evidence, characterized by en-echelon segments formed by centimetric open fractures and formed due to aseismic creep coeval or immediately subsequent to earthquakes along the Timpe Fault System and associated structures (e.g., the 1988, 2002, 2009 and 2018 seismic events). The deformation, characterized by prevalent right-lateral motion, is progressively attenuated to the east, where this structure seems to also accommodate movements of the Aci Catena and Aci Platani faults (Figure 2). According to Firetto-Carlino et al. [66], this structure extends offshore in the Ionian Sea, probably joining the Mt. Alfeo Fault System (see also [22]).

4. Geodetic Data

Since 1999, a GNSS (Global Navigation Satellite System) network has been realized at Mt. Etna [67] with the aim of monitoring ground deformation related to volcanic and tectonic processes. During the last two decades, many eruptive phases (inflation/deflation cycles), dike intrusions, sliding processes and tectonic displacements have been observed

and described (e.g., [30,36,61,67,68]). The analysis of ground deformation data has shown that the seaward sliding of the eastern flank of Mt. Etna is not constant over time, but accelerates during slow slip events, as observed in 2009, 2012 and 2016 [36,65,69] or after eruptions, as in 24 December 2018, when the south-eastward velocities of the unstable eastern flank increased drastically to values of about 300 mm/yr soon after the intrusion, with respect to values of about 30 mm/yr, of the pre-eruptive period [61]. These accelerations are the ideal phases for the kinematics of the fragmented flank of Mt. Etna to be investigated, as already shown in Monaco et al. [30].

As an example, in this work we analysed the shear strain rate pattern modelled between January and March 2017, during the increase in the velocities of the eastern flank associated with an inflation of the volcanic edifice. Indeed, from mid-2016, we observed a trend of inflation of the volcanic edifice (as already shown by Mattia et al. [61], highlighted by an areal dilatation of the triangle of the GNSS stations EDAM-EMEG-EINT (Figure 4A). It was interrupted by a brief period of areal contraction between the second half of March and the end of April 2017 due to eruptive activity at the summit craters. From January 2017 to just before the start of the eruptive activity, on March 2017, we observed an increase in the GNSS velocities along the unstable eastern flank of Mt. Etna, evidenced by the increase in the slope of the E–W components of the position time series (Figure 4B). For this short phase, we computed the velocity field (Figure 4C). The GNSS data were processed using the GAMIT/GLOBK software [70,71] with the strategy discussed in Mattia et al. (2020). The horizontal velocities showed a radial deformation pattern with greater values measured along the eastern flank Mt. Etna. During this phase of acceleration of the eastern flank, we inverted the GNSS horizontal velocity pattern to model the shear strain rate parameters. We applied the technique first introduced by Haines and Holt [72], improved by Holt and Haines [73] and applied to volcanic areas by Bruno et al. [67,69] for computing a spatially continuous strain rate. In this technique, an adjustable isotropic component of strain rate variance is considered as a measure of the a priori expected departure of strain rates from a long-term secular field. Such a departure would be a transient, associated for example with volcanic inflation. This single adjustable parameter is isotropic, and constant everywhere, because there is no a priori expectation on the style or distribution of the potential strain rate transient associated with volcanic deformation [72,74]. We designed a grid region surrounding Mt. Etna. The model was calculated on a regular $0.05^\circ \times 0.05^\circ$ grid, whose nodes did not coincide with any of the geodetic monuments and which extended from a longitude of 14.80° to 15.25° and a latitude of 37.50° to 37.90° .

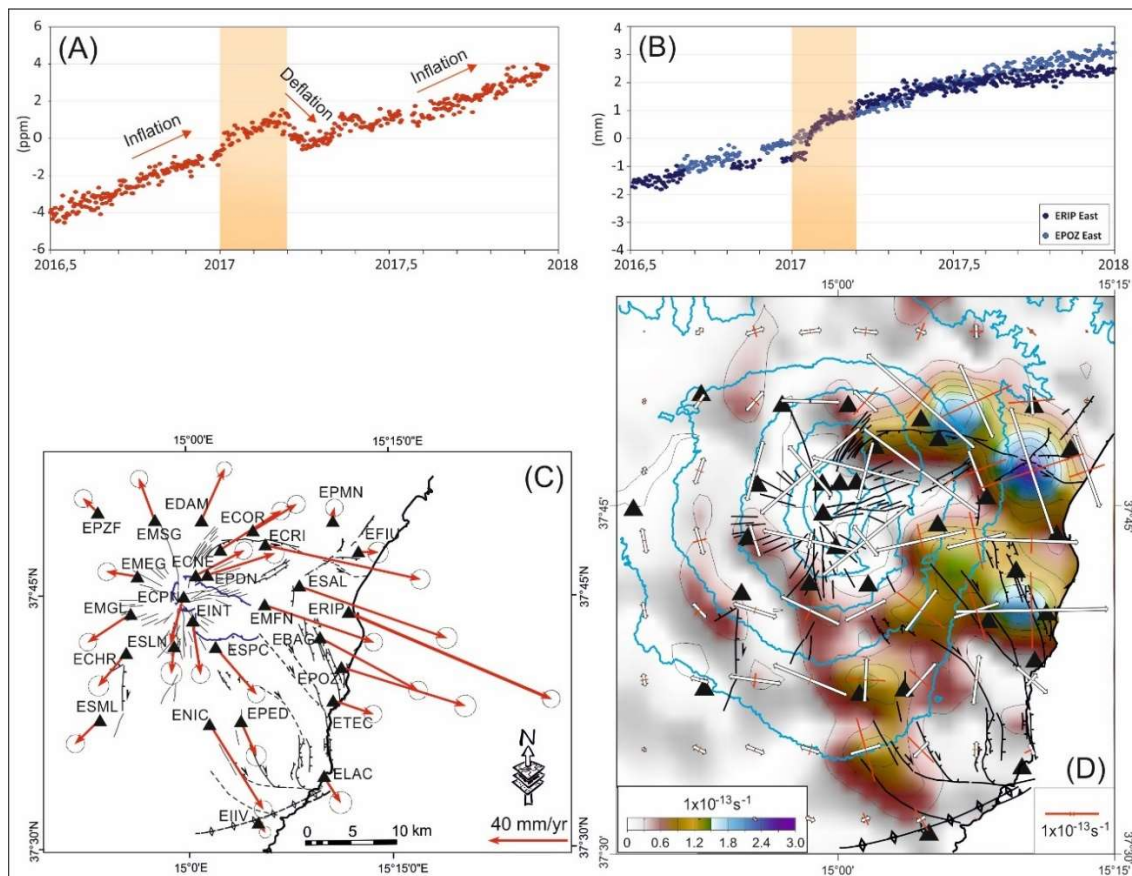


Figure 4. (A) Daily variation of the area recorded at an intermediate altitude triangle (EDAM-EMEG-EINT, see Figure 4C for GNSS station locations) from 1 July 2016 to the end of 2018. Positive variations (dilations) indicate inflation, while the negative variation (contraction) was measured during the deflation of the volcanic edifice due to volcanic activity. The orange rectangle highlights the time interval that we analyzed in this manuscript (1 January 2017–15 March 2017). (B) Daily E–W components of ERIP (blue points) and EPOZ (light blue points) GNSS stations on the eastern flank of Mount Etna (see Figure 4C for locations); (C) Measured GNSS horizontal velocities with 95% confidence ellipses for the period 1 January 2017–15 March 2017; (D) Geodetic shear strain rate at Mt. Etna associated with the component of the strain tensor field. Principal axes of the average strain rates within the 0.05×0.05 grid areas are reported in the eastern flank. Open arrows indicate extensional strain rates and solid red arrows correspond to compressional strain rates. The strain rate was modelled through the inversion of the GNSS velocities shown in Figure 4C. The black triangles indicate the GNSS stations.

As shown in Figure 4D, shear strain-rate variations up to $2.2 \times 10^{-13} \text{ s}^{-1}$ appeared during the January–March 2017 period of inflation of Mt. Etna in the area including the Fian-daca, Linera–Santa Tecla and S. Venerina faults and the Timpe Fault System. In this area, which represents the northern termination of the Alfeo–Etna shear zone, the geodetic shear strain rate associated with the component of the strain tensor field showed a pure strike-slip style of deformation resulting from equal magnitudes of the extensional and compressional principal axes. Meaningful variations of the shear strain rate along the Fian-daca, Linera–Santa Tecla and Santa Venerina faults have been already described for the period 14 June 2009–21 May 2010 (values up to $1.4 \times 10^{-13} \text{ s}^{-1}$) and 1 January–31 May 2019 (values up to $3.5 \times 10^{-13} \text{ s}^{-1}$), in Monaco et al. [30] and for the period 11 December 2015–17 May 2016 (values up to $1 \times 10^{-13} \text{ s}^{-1}$) in Bruno et al. [69], testifying to the importance of this structural alignment in the general context of the geodynamics of the Mt. Etna eastern flank. The variations confirms that this fault system is an important shear zone where the strain related to volcano-tectonic processes is accommodated and distributed along the weak and unconstrained eastern flank of Mt. Etna.

5. Marine Seismic Reflection Data

5.1. Data and Methods

The offshore realm was explored through a high-resolution seismic dataset consisting of seismic reflection lines sounded in the western Ionian Sea in the frame of the Poseidon expedition POS496 (Figure 5; R/V Meteor, March–April 2016, see also [75]). Seismic data were acquired using an 80-channel digital solid-state; a Geometrics GeoEel streamer with a group interval of 1.5625 m was used for seismic acquisition. A Sercel Mini GI-Gun seismic source, with a total volume of 0.4 L was shot in the harmonic mode. The shot interval was set to 6 s, resulting in a shot distance of ~12 m at a ship's speed of 4 knots.

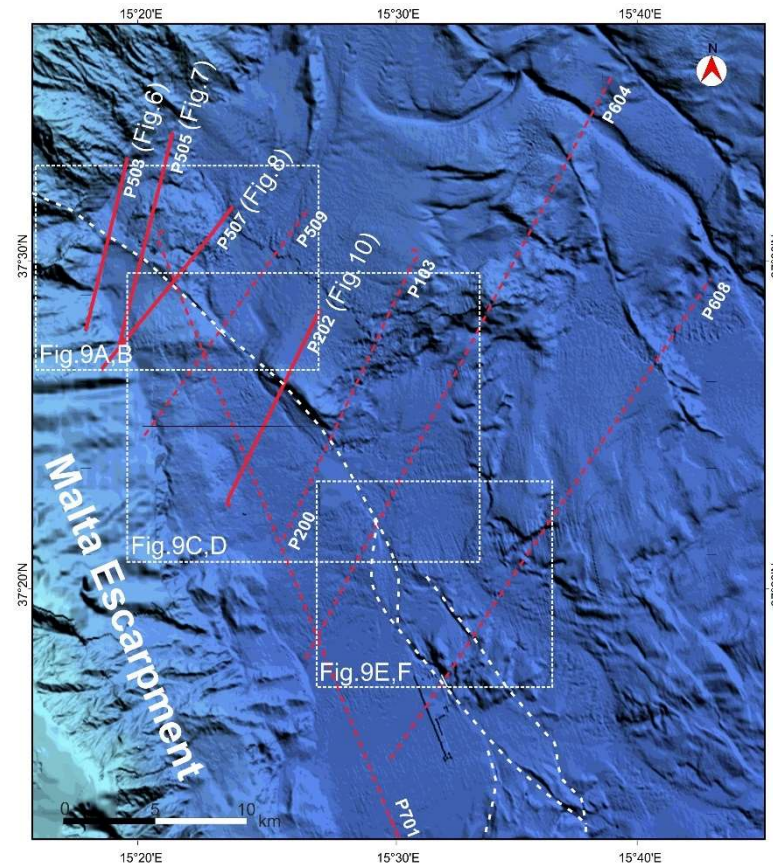


Figure 5. Seismic grid of the Poseidon expedition POS496 [75] in the Catania–Siracusa offshore (see location in Figure 1). Solid red lines are the profiles discussed in the text. The white dashed line is the trace of the North Alfeo Fault (from [10]).

The seismic profiles were processed using the commercial software package Schlumberger Vista Seismic Processing. The Processing workflow includes band-pass filtering with corner frequencies of 40/80/600/1000 Hz, despiking, debias filtering, Common Mid-Point (CMP) binning and Normal-Move-Out (NMO) correction. All data were time-migrated using the software's finite difference migration. Due to the relatively short streamer and the high water depths, no dedicated velocity analysis could be applied during NMO correction and migration. Hence, a constant velocity of 1500 m/s was applied. Moreover, previously published high-resolution bathymetric data [22,76] were consulted to better constrain the spatial extent of faults at the seafloor. A seismo-stratigraphic model available from nearby sectors was also considered to constrain the age of deformation (see [57] and Table 1). The interpretation was operated into the Move 2019.1 geo-modelling software package (Petex Ltd., Edinburgh, U.K.).

Table 1. Age and lithology of the seismic units occurring in the western Ionian area (from [57] and references therein).

Seismic Unit	Period	Age (Ma)	Lithology
PQ2	Quaternary	2.58–0.012	Silty sandstones
PQ1	Upper Pliocene	3.6–2.58	Silty sandstones
MES	Messinian	7.2–5.3	Evaporites
Pre-MES	Pre-Messinian	up to 7.2	Limestones

As regards the seismic stratigraphy of the western Ionian basin, we mainly referred to previous authors [57,77,78] that have provided a seismo-stratigraphic model in which four main seismic units are described (age and lithology are reported in Table 1). From the top to the bottom, they are the PQ2, PQ1 and MES units, representing the basin-fill units, and the Pre-MES unit that correlates to the carbonate bulk of the Malta Escarpment. The Pre-MES unit consists of a transparent seismic unit, interpreted as the acoustic basement. The MES unit consists of low- to medium-amplitude, generally subparallel, medium frequency reflectors. Its top reflector is represented by an irregular, erosive surface (S2 discontinuity of Gambino et al. [57]). The PQ1 unit is characterized by heterogeneous seismic facies consisting of a sequence of low- to high-amplitude, low to medium frequency, subparallel and continuous reflectors [57]. This unit includes wedge-shaped seismic bodies whereas its top reflector is often represented by an erosive surface above which the upper unit rests unconformably. Locally, a transparent seismic facies (PQ1a) is recognized below the PQ1 unit. Given its stratigraphic position, the PQ1a facies is interpreted as a Lower Pliocene deposit. The youngest PQ2 unit displays seismic facies made of high-frequency and high-amplitude reflectors with a good lateral continuity.

In the following section, we describe the main tectonic highlights of the northern sector of the Alfeo–Etna Fault System observed in high-resolution bathymetry (from [10,79]) and high-resolution seismic reflection lines crossing the shear zone (from Poseidon expedition POS496-R/V Meteor, March–April 2016, [75]).

5.2. The Offshore Tectonic Pattern

Four high-resolution seismic profiles (the P503, P505, P507 and P202, see Figure 5 for location), NNE–SSW-oriented and crossing transversally the Alfeo Fault System, were selected to describe the tectonic pattern of the abyssal plain located in the Mt. Etna offshore.

The P503 profile (Figure 6) passes through the fault zone at the foot of the continental slope about 15 km off Catania (see Figure 5 for location). Following the displaced reflectors and the deformation affecting the various seismic units, a positive flower structure, deforming a previous wedge-shaped extensional basin, has been reconstructed in the central portion of this seismic line. The structure is composed of a main sub-vertical fault surface and associated upward-diverging minor thrust faults (Figure 6). The associated reverse structures are more evident on the northern side of the main fault, where they have displaced the top-reflector of a highly reflective seismic unit. To the south of the main fault, the seismic stratigraphy can be reconstructed even if age attribution is difficult to operate. Seismic units are deformed according to the transpressional kinematics that characterize the fault zone in this sector.

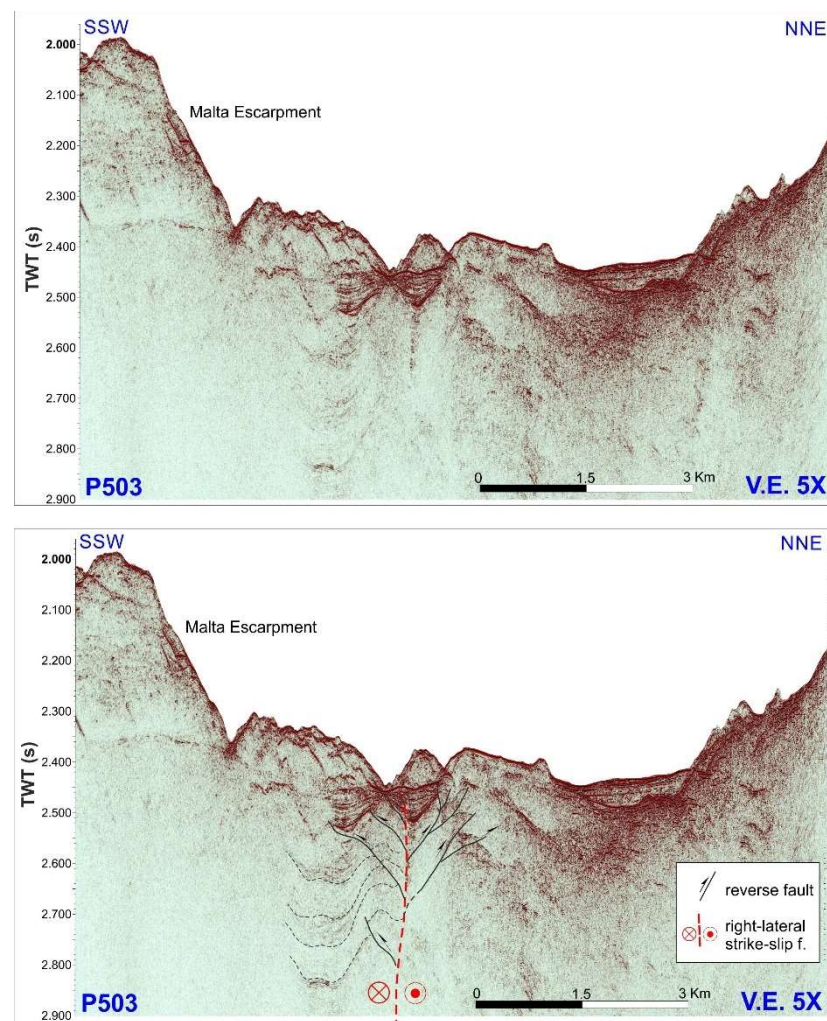


Figure 6. The p503 seismic profile and its interpretation below (see location in Figure 5).

The P505 profile (Figure 7) crosses the fault zone close to the foot of the continental slope, about 20 km off the coast of Catania (Figure 5). Here, the fault appears as a single sub-vertical structure deforming the entire sounded sub-seafloor seismo-stratigraphic setting. As suggested by reflectors bended-up approaching the tectonic structure, the fault zone is masked by an along-fault intrusion. Similar features have been observed in the western Ionian basin where they were interpreted as igneous [80,81] or serpentinitic/mud diapirs [82,83]. Notwithstanding, the different thickness of the PQ1 seismic unit on the two sides of the structure indicates that the offset associated to the fault zone is “out of the section”, and hence, mostly strike-slip.

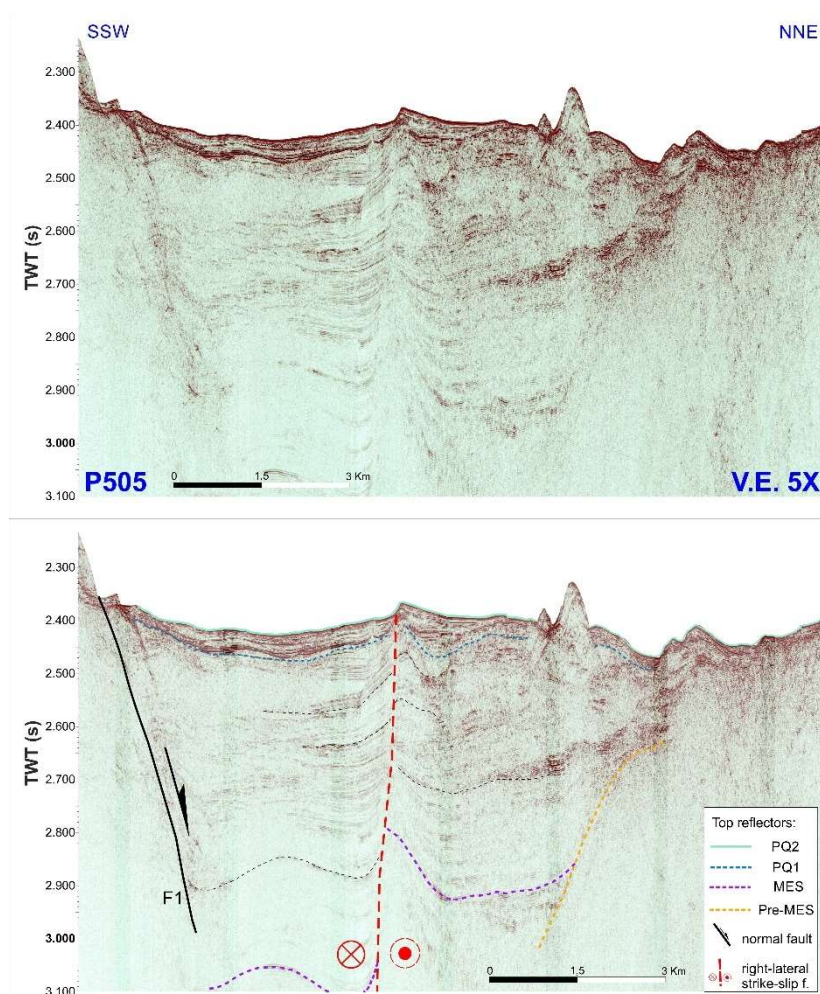


Figure 7. The p505 seismic profile and its interpretation below (see location in Figure 5).

The P507 profile (Figure 8) intercepts the fault zone a few km to the south-east (Figure 5). Following the illuminated seismo-stratigraphic section and the displaced reflectors, an asymmetric positive flower-structure can be interpreted along this line. The wrenching structure includes a sub-vertical (dip at roughly 85° to the NE) main fault, to which other minor faults, dipping with minor angles, seem to converge at depth. The propagation of the flower structure has displaced the sounded seismic units with a variable offset and the seafloor. At the southern side of the main fault, the thickness of sequences in the hanging wall is higher than in the footwall of the associated reverse faults, suggesting a tectonic inversion of a previous extensional pattern (Figure 8). The seafloor expression of the fault zone here consists of a lozenge-shaped bathymetric ridge (Figure 9A). According to the type of deformation observed in the seismic section, this bathymetric culmination can be interpreted as a restraining bend (*sensu* Woodcock and Fischer [84]) formed where the fault slightly changes its trajectory (Figure 9B).

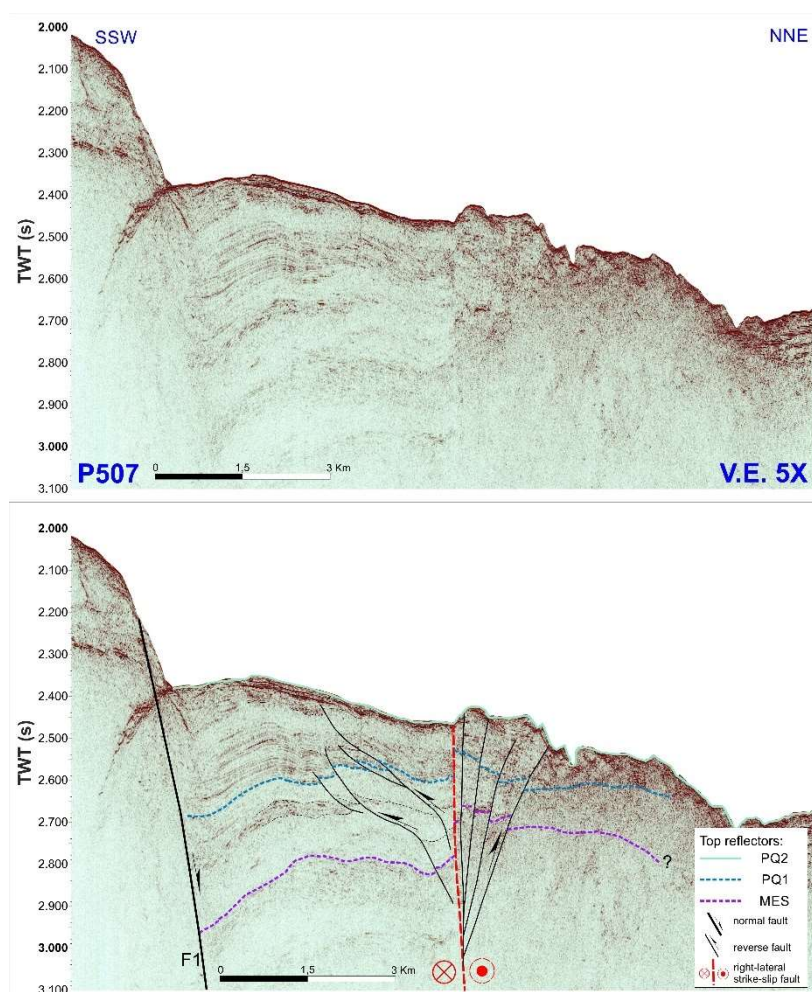


Figure 8. The p507 seismic profile and its interpretation below (see location in Figure 5).

The P202 profile (Figure 10) crosses the fault zone to the southeast (Figure 5); along this section, the tectonic expression of the fault is not clearly detectable since the fault zone is again masked by the along-fault upraise of diapiric material [80–83]. Nevertheless, the not-resolved fault pattern in the seismic section appears more evident at the seafloor where the shear zone shows a clear bathymetric expression (Figure 9C). This consists of a sigmoidal-shaped, 5 km long bathymetric culmination with a steep scarp on its southwestern slope. The culmination probably results from a combination of a seafloor dome structure, produced by the uprising diapiric material, subsequently displaced by the later propagation of a transtensional structure (Figure 9D).

Another transtensional feature, interpreted as a pull-apart basin related to dextral strike-slip kinematics by Gutscher et al. [10], is clearly detectable by bathymetric expression to the south-east (Figure 9E). In our opinion, such a structure is related to a releasing bend (*sensu* Woodcock and Fischer [84]) (Figure 9F).

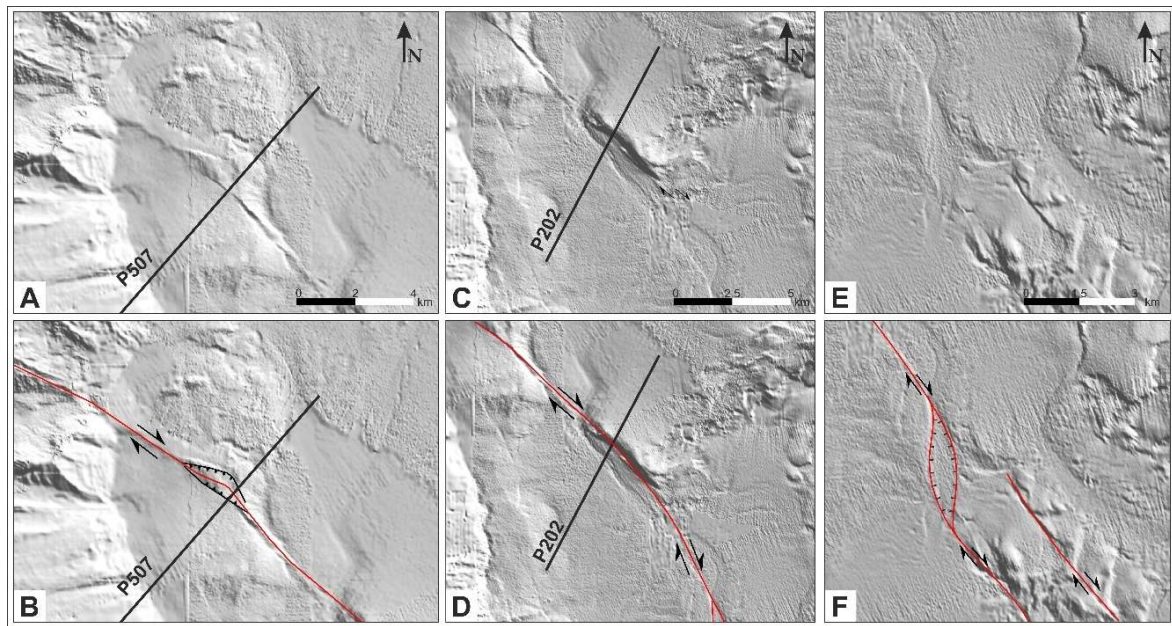


Figure 9. Morphostructural features along the North Alfeo Fault: restraining bend (A,B), diapir-related (C,D) and releasing bend (E,F) geometries (see location in Figure 5).

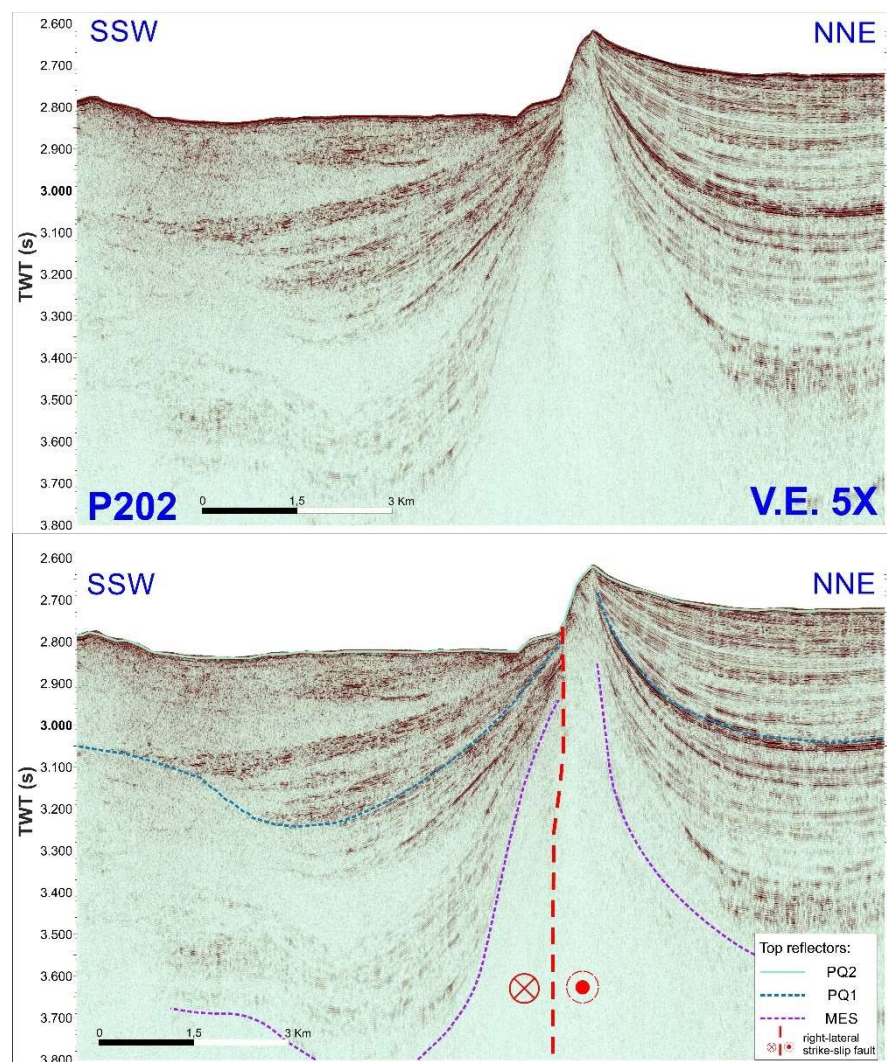


Figure 10. The p202 seismic profile and its interpretation below (see location in Figure 5).

6. Seismological Data

The seismic pattern of the last 40 years has been investigated by referring to the catalogues available by the Istituto Nazionale di Geofisica e Vulcanologia, which contain instrumental observations of the seismic activity in Italy since the 1980s (see <https://istituto.ingv.it/it/risorse-e-servizi/archivi-e-banche-dati.html>, accessed on 13 January 2022; <https://www.ct.ingv.it/index.php/monitoraggio-e-sorveglianza/banche-dati-terremoti/terremoti>, accessed on 13 January 2022). In the coastal area of south-eastern Sicily and the Ionian Sea (Figure 11), recorded earthquakes have a magnitude mostly between 1 and 4; the two strongest events occurred on 13 December 1990 (M_L 5.4), in the near Ionian offshore, about 20 km SSE of Catania [85] and on 26 December 2018 (M_w 4.9) in relation to the Fiandaca fault on Mt. Etna (e.g., [30]).

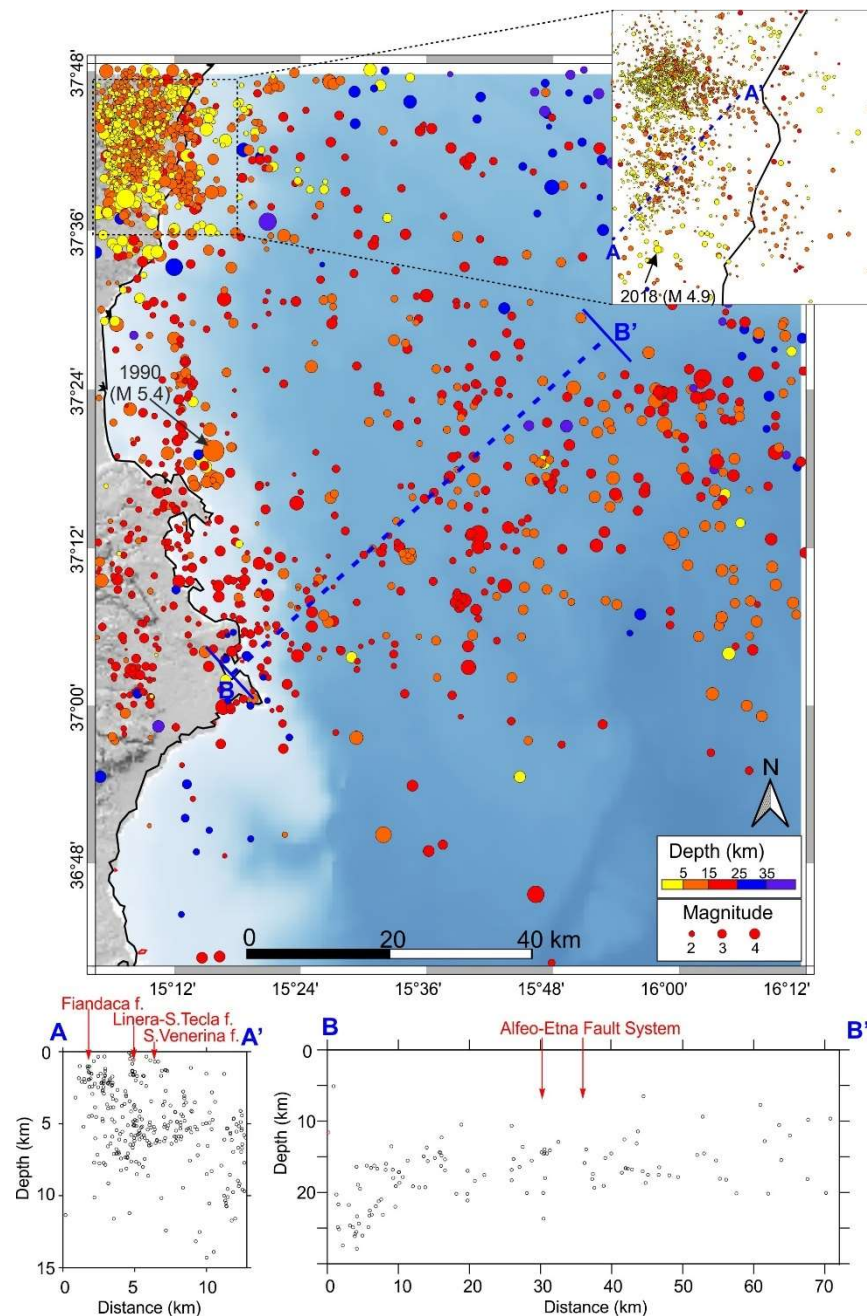


Figure 11. Final location on the map and the vertical sections of the last 40 years seismic events (see text). Cross sections (marked in map) incorporate all relocated events within ± 3 km (AA') and ± 6 km (BB') from the cross-section lines.

In order to improve the quality of the seismic dataset, the events selected in the Ionian Sea and in the eastern flank of Mt. Etna areas were relocated using the tomoDDPS code [86] with the 3D velocity model by Scarfi et al. [30]. The map with the final locations is shown in Figure 11. Most of the seismicity is concentrated in the Mt. Etna area; specifically, the events are located along the Fiandaca, Linera–S. Tecla and S. Venerina faults and the Timpe Fault System. The typical seismogenic depth is shallow, down to 6–8 km. In the Ionian Sea the seismicity appears more scattered, even if some alignments along the main structures are noticed in relation to the central–southern sector of the Alfeo-Etna Fault System. In this area, the hypocentral depth is between 10 and 25 km. In the southernmost sector, earthquakes are scarce; however, this could partly be due to the lower detection capability of the seismic network, due to the large gap in the offshore.

The kinematics of the area, deduced from the data collected by Scarfi et al. [40], are predominantly strike-slip (Figure 12A), with right-lateral movements along planes striking from WNW–ESE to NW–SE and with NNW–SSE horizontal P-axes (Figure 12B,C). As a whole, the seismological data confirm the occurrence of right-lateral shearing and associated structures along a fault zone extending from Mt. Etna to the Alfeo Sea Mount (Figures 1 and 13).

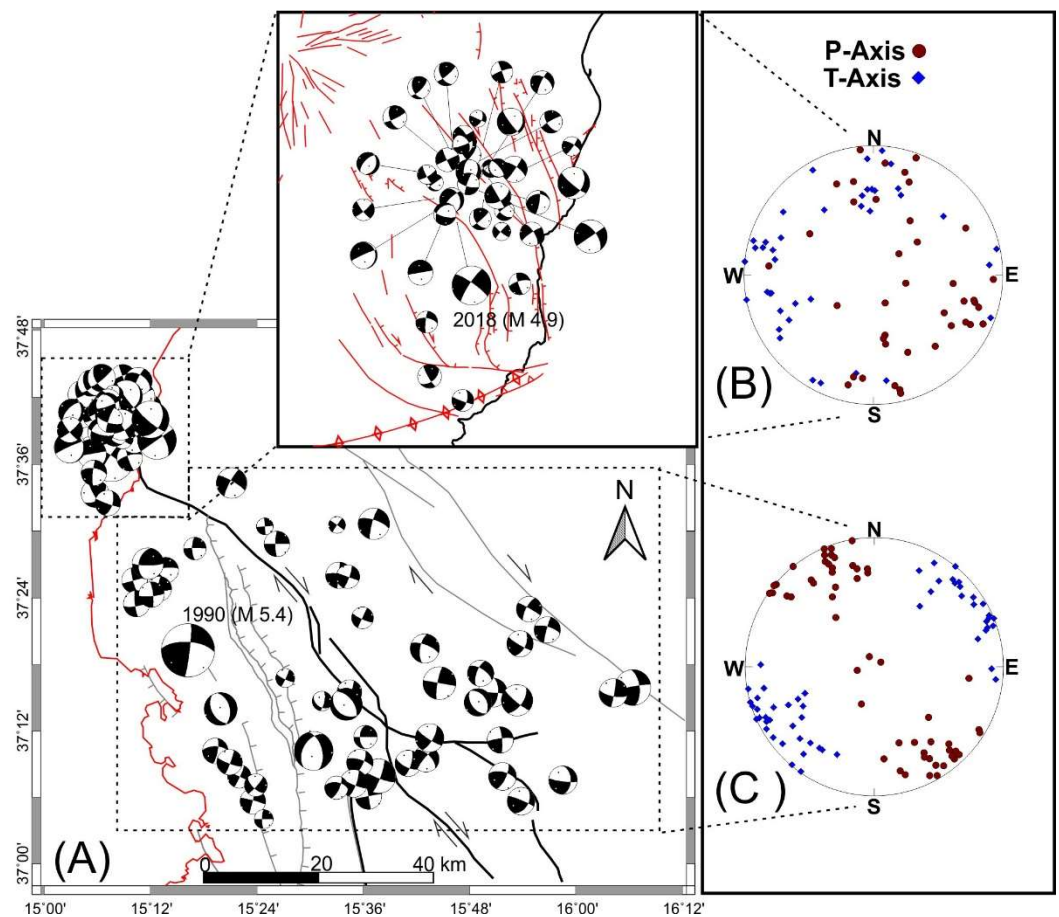


Figure 12. (A) Map showing the focal solutions deduced from data collected by Scarfi et al. [40]. Diagrams (B) and (C) show P–T axes distribution in the Etnean and Ionian areas, respectively.

7. Data Analysis

Morpho-structural field data integrated with marine geophysical data and compared with geodetic shear strain rates and recent seismicity show the occurrence of a roughly NW–SE-oriented dextral shear zone extending from the south-eastern flank of Mt. Etna to the Alfeo Sea Mount (Figure 1).

Morpho-structural field data, mostly deriving from our previous research (see [2–5,9–11,18,22,28,33,36,42,47,55,65]) integrated with data from the literature (see Section 3) have been reinterpreted in the light of the definition of a unique tectonic belt that extends from the south-eastern slope of Mt. Etna to the offshore (Figure 13). The NW–SE-trending tectonic structures occurring in the lower south-eastern slope of Mt. Etna (i.e., the Fiandaca, Linera–Santa Tecla and Santa Venerina faults), are connected to the major Alfeo–Etna Fault System, whose activity characterizes the western Ionian offshore, through the Acireale and Aci Catena faults belonging to the Timpe Fault System (Figure 2). This is characterized by NNW–SSE to N–S-trending segments, and by minor associated extensional joints [87], resulting from an ~ E–W-oriented extension. The N–S-oriented segments show dip-slip motion, the NNW–SSE-oriented faults show a minor oblique-dextral component of motion, while the NW–SE-oriented segments, such as the Fiandaca fault, reactivated on 26 December 2018, show right-lateral transcurrent movements with associated en-echelon N–S-oriented open fractures. All the analysed structures are seismically active, having given rise to shallow and low magnitude earthquakes in the last 150 years. In turn, the NW–SE-trending shear zone, including the Fiandaca, Linera–Santa Tecla and Santa Venerina faults and other minor faults, connects the Timpe Fault System, characterized by prevalent normal faulting, with the upper slope of the volcano, where the eruptive activity mostly occurs along two major linked rift zones (Figures 2 and 13; [2,6,18]).

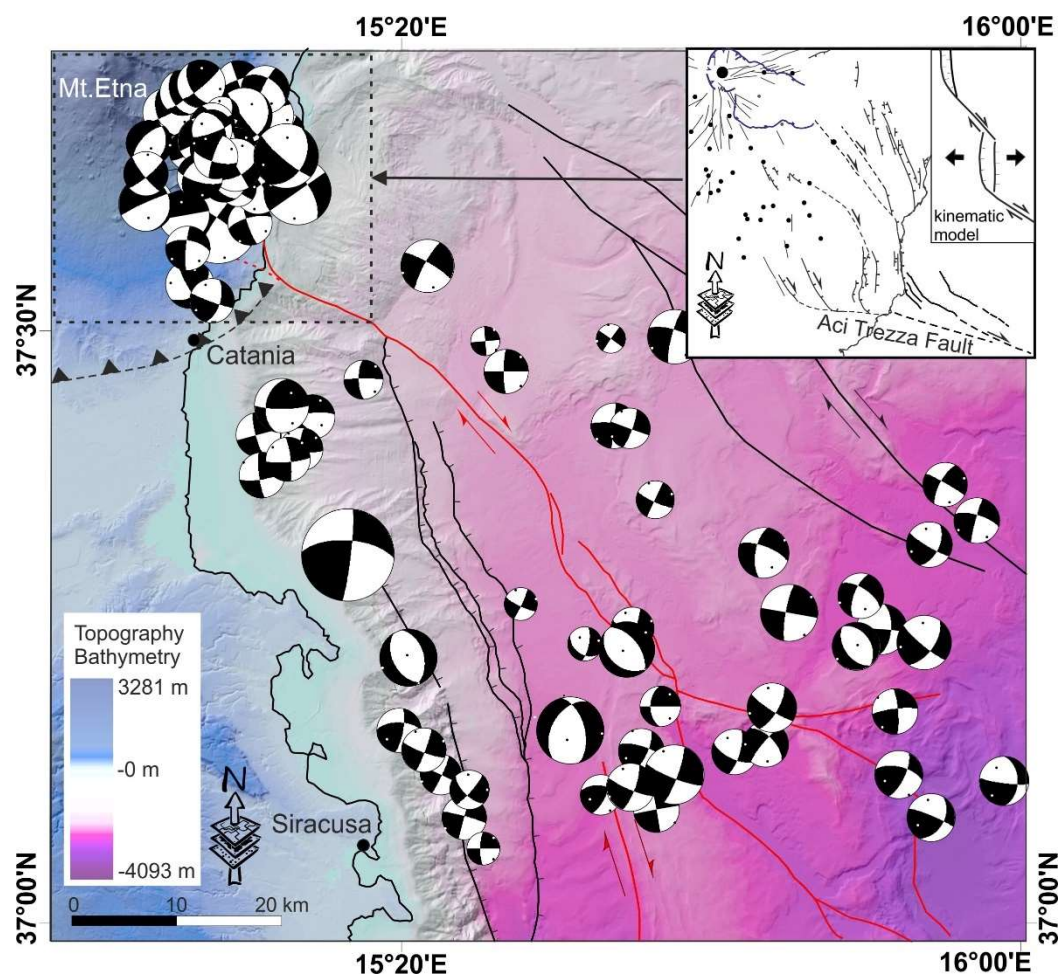


Figure 13. Seismotectonic map of the western Ionian Sea and Mt. Etna area. The Alfeo–Etna faults (after [9,10,47]) are red colored (see Figure 1 for location). Inset shows the kinematic interpretation of the volcano-tectonic structures (see Figures 1 and 2 for the legend) occurring in the eastern sector of Mt. Etna in the framework of the Alfeo–Etna shear zone (releasing sectors, see [84,88–90]).

The geodetic GNSS data of the Mt. Etna permanent network for the period 2009–2018 (see Section 4 and [26,67,69]) show the orientation of the principal axes of the average strain rates (Figure 4D) that are compatible with the field data and focal solutions of the seismic events. Moreover, “significant” shear strain rate values were measured in the area of the Fiandaca, Linera–Santa Tecla and S. Venerina faults during the phases in which an increase in the velocities of the GNSS stations was measured. In particular, for the phase analysed in this manuscript (January–March 2017), we measured values of about $2.2 \times 10^{-13} \text{ s}^{-1}$. These values are similar to those modelled in 2009–2010 and are slightly lower than the values obtained in the first months of 2019, after the $M = 4.9$ Fiandaca earthquake [26].

Finally, new multichannel seismic profiles (see Section 5), compared with data derived in the bathyal plain from published multibeam bathymetry (see [22,79]), clearly confirm the occurrence of a NW–SE-trending dextral shear zone in the offshore (see also [21–23]), extending between Mt. Etna and the Alfeo Sea Mount (Figure 13), characterized by recent reactivations clearly recorded by sea-bottom morphology (Figures 5 and 9). A new accurate space–time analysis of recent seismicity (period 1980–2020, Section 6, Figure 11) allows the seismological features and the prevalent right-lateral transtensive kinematics of the Alfeo–Etna shear zone to be defined (Figures 12 and 13). It is characterized by diffused seismicity with seismic clusters in the south-eastern slope of the volcano and at its southern termination. In general, focal solutions show compressive and strike-slip fault mechanisms characterized by NNW–SSE-striking horizontal P-axes, as well as rare extensional events along the NNE–SSW-oriented plane, with horizontal T-axes striking ~E–W. The coexistence of different mechanisms of deformation is compatible with low differential stresses at releasing sectors of strike-slip faults [88].

8. Discussion and Conclusions

Seismic profiles, seismological data and bathymetric maps (see also [21,22,47,79]) suggest that the shear zone occurring in the Ionian offshore (the Alfeo–Etna Fault System) also affects the eastern flank of the volcano with the same kinematics (Figures 2 and 13). Our data coherently indicate that the NW–SE-trending oblique dextral fault system of the Alfeo–Etna Fault System turns to the N–S direction near the Ionian coastline, where the Timpe Fault System occurs, and continues up-slope connecting to the Fiandaca, Linera–Santa Tecla and S. Venerina faults, forming, as a whole, a releasing bend zone (sensu Woodcock and Fischer [84]). Along this major tectonic alignment, crustal structures such as releasing bends and stepovers (sensu Woodcock and Schubert [89]) both occur offshore and are clearly related to the dextral motion of the shear zone (see also [22]). It is worth noting that although no strong historical earthquake occurred in the releasing sector along the Mt. Etna coastline, it was strongly active during the Late Pleistocene–Holocene. This is evident in the footwall uplift of the Acireale fault, with rates up to 3–4 mm/yr [14,55] and/or by several creep events along the Aci Catena fault [63]. Therefore, it is a potential seismogenic sector where strong earthquakes could occur in the future.

In the upper sector of the Etnean volcanic edifice (Figures 2 and 13), the extensional component at the ends of the NW–SE-trending shear zone is accommodated by rift zones [3–5,7] that could represent terminal extension fractures of dextral strike-slip faults (sensu Sylvester [90]). In particular, the Southern Rift, where the major fissural eruptions in the last 15 ka occurred [2,6], is connected to the Alfeo–Etna shear zone by the Tremestieri and Tre-castagni seismogenic faults through the aseismic Aci Trezza transfer fault (Figures 2 and 13). This study confirms our previous findings about the recent deformation of the eastern flank of Mt. Etna (see [33]): in our interpretation, crustal tectonic processes related to the geodynamics of the western Ionian Sea are predominant and prevail over the gravitational instability. In fact, as demonstrated by Mattia et al. [33], the aseismic gravitational sliding of the shallowest stratigraphic level of the eastern flank of Mt. Etna has only recently superimposed on the long-term volcano–tectonic activity and regional uplifting [55,91]. Slow-slip and creep events that reactivate the structures between the tectonic blocks are

accommodated by a low-angle and shallow crustal discontinuity limited southwards by the Acì Trezza fault [65], that aseismically joins the Alfeo–Etna faults (Figure 12).

It is worth noting that the south-eastern sector of the volcano is the site of one of the main pathways for magma uprising from depth [92–96]. In this regard, we may consider that among the many monogenetic pyroclastic cones that constellate the flanks of the Etnean edifice, the most numerous and voluminous are located in the south-eastern sector (see also [97]) between the Southern Rift and the Tremestieri and Trecastagni faults (Figure 2). At the Mt. Etna volcano, the monogenic cones are formed during eruptions that most of the time are mixed, effusive and explosive [98]. According to our past research [99–101], the size of the cones is directly related to the accumulation of fragmented magma as result of the magnitude of the explosive fraction of the eruptive event, which in turn is associated with the amount of gas within the magma feeding it. Consequently, it could be argued that the large spatter cones in the south-eastern sector of the volcano, more numerous than in the other sectors, derive their size from their association with the eruptive events of voluminous batches of gas rich magma. This suggests that the erupted magma could not have degassed through the central axis connected to the summit craters, which, in other words, indicates that the magma rose through conduits independent from the system feeding the central axis. Following this reasoning (see also [97,102] for an in-depth analysis), we must admit that the tectonic processes able to set up a feeding system independent from the central axis occur in the south-eastern sector of Mt. Etna. A deformation model that could be envisaged to justify such an occurrence associated with the Alfeo–Etna shear zone is the triggering of local transtension capable of giving rise to small pull-aparts and/or releasing bends at which fractures (see also [3]) could allow the rise of fluids and work as autonomous magma feeding systems. Similar relations between strike-slip faulting and volcanism have been observed in other volcanic areas all over the world (e.g., [102–106]). Although these observations deserve future studies, volcanological evidence indicates the fundamental importance of strike-slip tectonics in the evolution of the Etnean volcanic region and in general confirms the primary role of tectonics in Mt. Etna volcanism.

Author Contributions: S.G. and C.M.: Conceptualization, Investigation, Methodology, Writing—original draft, Writing—review and editing, Data curation, Supervision. G.B., V.B., C.F., M.M. and L.S.: Investigation, Formal analysis, Methodology, Writing—original draft, Data curation, Visualization. G.D.G., F.G. Investigation, Formal analysis, Methodology, Data curation, Visualization. All authors have read and agreed to the published version of the manuscript.

Funding: This research was funded by the Catania University PIA.CE.RI. Project (linea 2) “Interaction between volcanic activity and active tectonic processes in the Mt. Etna area (InvultEtna). The research has moreover benefited from funding provided by the agreement between Istituto Nazionale di Geofisica e Vulcanologia (INGV) and the Italian Presidenza del Consiglio dei Ministri, Dipartimento della Protezione Civile (DPC—Presidency of the Council of Ministers—Italian Civil Protection Department). This paper does not necessarily represent DPC official opinion and Policies.

Institutional Review Board Statement: Not applicable.

Informed Consent Statement: Not applicable.

Data Availability Statement: See text for links to publicly archived datasets analysed. Data supporting reported results are available on request by email to the corresponding author (cmonaco@unict.it).

Acknowledgments: Daniele Cirillo and other three anonymous reviewers are kindly acknowledged for their constructive comments and suggestions. The research was also performed in the frame of the PRIN 2017-MUSE 4D project—Overtime tectonic, dynamic and rheologic control on destructive multiple seismic events—Special Italian Faults and Earthquakes: from real 4D cases to models. The authors acknowledge the use of Daisy3 Software by Francesco Salvini (University of Roma3) and of MOVE Software Suite granted by Petroleum Experts Limited (www.petex.com, accessed on 13 January 2022). This work is part of the S. Gambino. research project at the University of Catania.

Conflicts of Interest: The authors declare no conflict of interest.

References

1. Branca, S.; Coltelli, M.; De Beni, E.; Wijbrans, J. Geological evolution of Mount Etna volcano (Italy) from earliest products until the first central volcanism (between 500 and 100 ka ago) inferred from geochronological and stratigraphic data. *Geol. Rundsch.* **2007**, *97*, 135–152. <https://doi.org/10.1007/s00531-006-0152-0>.
2. Barreca, G.; Branca, S.; Monaco, C. Three-Dimensional Modeling of Mount Etna Volcano: Volume Assessment, Trend of Eruption Rates, and Geodynamic Significance. *Tectonics* **2018**, *37*, 842–857. <https://doi.org/10.1002/2017tc004851>.
3. Monaco, C.; Tapponnier, P.; Tortorici, L.; Gillot, P.Y. Late Quaternary slip rates on the Acireale-Piedimonte normal faults and tectonic origin of Mt. Etna (Sicily). *Earth Planet. Sci. Lett.* **1997**, *147*, 125–139.
4. Giacomoni, P.P.; Ferlito, C.; Alesci, G.; Coltorti, M.; Monaco, C.; Viccaro, M.; Cristofolini, R. A common feeding system of the NE and S rifts as revealed by the bilateral 2002/2003 eruptive event at Mt. Etna (Sicily, Italy). *Bull. Volcanol.* **2012**, *74*, 2415–2433. <https://doi.org/10.1007/s00445-012-0672-3>.
5. Bruno, V.; Ferlito, C.; Mattia, M.; Monaco, C.; Rossi, M.; Scandura, D. Evidence of a shallow magma intrusion beneath the NE Rift system of Mt. Etna during 2013. *Terra Nova* **2016**, *28*, 356–363. <https://doi.org/10.1111/ter.12228>.
6. Branca, S.; Coltelli, M.; Gropelli, G.; Lentini, F. Geological map of Etna volcano, 1:50,000 scale. *Ital. J. Geosci.* **2011**, *130*, 265–291. <https://doi.org/10.3301/ijg.2011.15>.
7. Monaco, C.; Catalano, S.; Cocina, O.; De Guidi, G.; Ferlito, C.; Gresta, S.; Musumeci, C.; Tortorici, L. Tectonic control on the eruptive dynamics at Mt. Etna volcano (eastern Sicily during the 2001 and 2002–2003 eruptions). *J. Volcanol. Geother. Res.* **2005**, *144*, 221–233.
8. Gambino, S.; Barreca, G.; Gross, F.; Monaco, C.; Gutscher, M.; Alsop, G.I. Assessing the rate of crustal extension by 2D sequential restoration analysis: A case study from the active portion of the Malta escarpment. *Basin Res.* **2022**, *34*, 321–341. <https://doi.org/10.1111/bre.12621>.
9. Polonia, A.; Torelli, L.; Artoni, A.; Carlini, M.; Faccenna, C.; Ferranti, L.; Gasperini, L.; Govers, R.; Klaeschen, D.; Monaco, C.; et al. The Ionian and Alfeo–Etna fault zones: New segments of an evolving plate boundary in the central Mediterranean Sea? *Tectonophysics* **2016**, *675*, 69–90. <https://doi.org/10.1016/j.tecto.2016.03.016>.
10. Gutscher, M.-A.; Dominguez, S.; de Lepinay, B.M.; Pinheiro, L.; Gallais, F.; Babonneau, N.; Cattaneo, A.; Le Faou, Y.; Barreca, G.; Micallef, A.; et al. Tectonic expression of an active slab tear from high-resolution seismic and bathymetric data offshore Sicily (Ionian Sea). *Tectonics* **2016**, *35*, 39–54. <https://doi.org/10.1002/2015tc003898>.
11. Palano, M.; Ferranti, L.; Monaco, C.; Mattia, M.; Aloisi, M.; Bruno, V.; Cannavò, F.; Siligato, G. GPS velocity and strain fields in Sicily and southern Calabria, Italy: Updated geodetic constraints on tectonic block interaction in the central Mediterranean. *J. Geophys. Res. Earth Surf.* **2012**, *117*, 07401. <https://doi.org/10.1029/2012jb009254>.
12. De Guidi, G.; Lanzafame, G.; Palano, M.; Puglisi, G.; Scaltrito, A.; Scarfi, L. Multidisciplinary study of the Tindari Fault (Sicily, Italy) separating ongoing contractional and extensional compartments along the active Africa–Eurasia convergent boundary. *Tectonophysics* **2013**, *588*, 1–17. <https://doi.org/10.1016/j.tecto.2012.11.021>.
13. D’Agostino, N.; Selvaggi, G. Crustal motion along the Eurasia–Nubia plate boundary in the Calabrian Arc and Sicily and active extension in the Messina Straits from GPS measurements. *J. Geophys. Res. Earth Surf.* **2004**, *109*. <https://doi.org/10.1029/2004jb002998>.
14. Serpelloni, E.; Bürgmann, R.; Anzidei, M.; Baldi, P.; Ventura, B.M.; Boschi, E. Strain accumulation across the Messina Straits and kinematics of Sicily and Calabria from GPS data and dislocation modeling. *Earth Planet. Sci. Lett.* **2010**, *298*, 347–360. <https://doi.org/10.1016/j.epsl.2010.08.005>.
15. Lo Giudice, E.; Rasà, R. Very shallow earthquakes and brittle deformation in active volcanic areas: The Etnan region as an example. *Tectonophysics* **1992**, *202*, 257–262.
16. De Guidi, G.; Brighenti, F.; Carnemolla, F.; Cataldo, D.; Piro, A.G. New rapid vertical deformation of Santa Tecla Fault scarp (Mt. Etna volcano, Sicily) by lichenometry method. *Quaternary Int.* **2019**, *525*, 78–88. <https://doi.org/10.1016/j.quaint.2019.07.031>.
17. Gresta, S.; Bella, D.; Musumeci, C.; Carveni, P. Some efforts on active faulting processes (earthquake and aseismic creep) acting on the eastern flank of Mt. Etna (Sicily). *Acta Vulcanol.* **1997**, *9*, 101–107.
18. Monaco, C.; De Guidi, G.; Ferlito, C. The Morphotectonic map of Mt. Etna. *Ital. J. Geosci.* **2010**, *129*, 408–428. <https://doi.org/10.3301/ijg.2010.11>.
19. Azzaro, R. Earthquake surface faulting at Mount Etna volcano (Sicily) and implications for active tectonics. *J. Geodyn.* **1999**, *28*, 193–213. [https://doi.org/10.1016/s0264-3707\(98\)00037-4](https://doi.org/10.1016/s0264-3707(98)00037-4).
20. Azzaro, R. Seismicity and Active Tectonics in the Etna Region: Constraints for a Seismotectonic Model. In *Mt. Etna: Volcano Laboratory*; Geophysical Monograph Series; Bonaccorso, A., Calvari, S., Coltelli, M., Del Negro, C., Falsaperla, S., Eds.; AGU: Washington, DC, USA, 2004; Volume 143, pp. 205–220.
21. Azzaro, R.; Branca, S.; Gwinner, K.; Coltelli, M. The volcano-tectonic map of Etna volcano, 1:100,000 scale: An integrated approach based on a morphotectonic analysis from high-resolution DEM constrained by geologic, active faulting and seismotectonic data. *Ital. J. Geosci.* **2012**, *131*, 153–170. <https://doi.org/10.3301/ijg.2011.29>.
22. Barreca, G.; Bonforte, A.; Neri, M. A pilot GIS database of active faults of Mt. Etna (Sicily): A tool for integrated hazard evaluation. *J. Volcanol. Geotherm. Res.* **2013**, *251*, 170–186. <https://doi.org/10.1016/j.jvolgeores.2012.08.013>.
23. Hirn, A.; Nicolich, R.; Gallart, J.; Laigle, M.; Cernobori, L.; ETNASEIS Scientific Group. Roots of Etna volcano in faults of great earthquakes. *Earth Planet. Sci. Lett.* **1997**, *148*, 171–191. [https://doi.org/10.1016/s0012-821x\(97\)00023-x](https://doi.org/10.1016/s0012-821x(97)00023-x).

24. Gvirtzman, Z.; Nur, A. The formation of Mount Etna as the consequence of slab rollback. *Nature* **1999**, *401*, 782–785. <https://doi.org/10.1038/44555>.
25. Doglioni, C.; Innocenti, F.; Mariotti, G. Why Mt Etna? *Terra Nova* **2001**, *13*, 25–31.
26. Argnani, A.; Mazzarini, F.; Bonazzi, C.; Bisson, M.; Isola, I. The deformation offshore of Mount Etna as imaged by multichannel seismic reflection profiles. *J. Volcanol. Geotherm. Res.* **2013**, *251*, 50–64. <https://doi.org/10.1016/j.jvolgeores.2012.04.016>.
27. Maesano, F.E.; Tiberti, M.M.; Basili, R. Deformation and Fault Propagation at the Lateral Termination of a Subduction Zone: The Alfeo Fault System in the Calabrian Arc, Southern Italy. *Front. Earth Sci.* **2020**, *8*, 107. <https://doi.org/10.3389/feart.2020.00107>.
28. Barreca, G.; Branca, S.; Corsaro, R.A.; Scarfi, L.; Cannavò, F.; Aloisi, M.; Monaco, C.; Faccenna, C. Slab Detachment, Mantle Flow, and Crustal Collision in Eastern Sicily (Southern Italy): Implications on Mount Etna Volcanism. *Tectonics* **2020**, *39*, e2020TC006188. <https://doi.org/10.1029/2020tc006188>.
29. SgROI, T.; Polonia, A.; Barberi, G.; Billi, A.; Gasperini, L. New seismological data from the Calabrian arc reveal arc-orthogonal extension across the subduction zone. *Sci. Rep.* **2021**, *11*, 473. <https://doi.org/10.1038/s41598-020-79719-8>.
30. Monaco, C.; Barreca, G.; Bella, D.; Brighenti, F.; Bruno, V.; Carnemolla, F.; De Guidi, G.; Mattia, M.; Menichetti, M.; Roccheggiani, M.; et al. The seismogenic source of the 2018 December 26th earthquake (Mt. Etna, Italy): A shear zone in the unstable eastern flank of the volcano. *J. Geodyn.* **2021**, *143*, 101807. <https://doi.org/10.1016/j.jog.2020.101807>.
31. SgROI, T.; Lavecchia, G.; De Nardis, R. Crustal structure and seismotectonics of central Sicily (southern Italy): New constraints from instrumental seismicity. *Geophys. J. Int.* **2012**, *189*, 1237–1252. <https://doi.org/10.1111/j.1365-246x.2012.05392.x>.
32. De Guidi, G.; Barberi, G.; Barreca, G.; Bruno, V.; Cultrera, F.; Grassi, S.; Imposa, S.; Mattia, M.; Monaco, C.; Scarfi, L.; et al. Geological, seismological and geodetic evidence of active thrusting and folding south of Mt. Etna (eastern Sicily): Reevaluation of “seismic efficiency” of the Sicilian Basal Thrust. *J. Geodyn.* **2015**, *90*, 32–41. <https://doi.org/10.1016/j.jog.2015.06.001>.
33. Scarfi, L.; Barberi, G.; Barreca, G.; Cannavò, F.; Koulakov, I.; Patanè, D. Slab narrowing in the Central Mediterranean: The Calabro-Ionian subduction zone as imaged by high resolution seismic tomography. *Sci. Rep.* **2018**, *8*, 5178. <https://doi.org/10.1038/s41598-018-23543-8>.
34. Barreca, G.; Scarfi, L.; Gross, F.; Monaco, C.; De Guidi, G. Fault pattern and seismotectonic potential at the south-western edge of the Ionian Subduction system (southern Italy): New field and geophysical constraints. *Tectonophysics* **2019**, *761*, 31–45. <https://doi.org/10.1016/j.tecto.2019.04.020>.
35. Azzaro, R.; Bonforte, A.; Branca, S.; Guglielmino, F. Geometry and kinematics of the fault systems controlling the unstable flank of Etna volcano (Sicily). *J. Volcanol. Geotherm. Res.* **2013**, *251*, 5–15. <https://doi.org/10.1016/j.jvolgeores.2012.10.001>.
36. Mattia, M.; Bruno, V.; Caltabiano, T.; Cannata, A.; Cannavò, F.; D’Alessandro, W.; Di Grazia, G.; Federico, C.; Giammanco, S.; La Spina, A.; et al. A comprehensive interpretative model of slow slip events on Mt. Etna’s eastern flank. *Geochem. Geophys. Geosystems* **2015**, *16*, 635–658. <https://doi.org/10.1002/2014gc005585>.
37. Corsaro, R.A.; Neri, M.; Pompilio, M. Paleo-environmental and volcano-tectonic evolution of the southern flank of Mt. Etna during the last 225 ka inferred from the volcanic succession of the «Timpe», Acireale, Sicily. *J. Volcanol. Geother. Res.* **2002**, *113*, 289–306.
38. Azzaro, R.; D’Amico, S.; Tuvè, T. Estimating the Magnitude of Historical Earthquakes from Macroseismic Intensity Data: New Relationships for the Volcanic Region of Mount Etna (Italy). *Seism. Res. Lett.* **2011**, *82*, 533–544. <https://doi.org/10.1785/gssrl.82.4.533>.
39. Scarfi, L.; Messina, A.; Cassisi, C. Sicily and southern Calabria focal mechanism database: A valuable tool for local and regional stress-field determination. *Ann. Geophys.* **2013**, *56*, D0109. <https://doi.org/10.4401/ag-6109>.
40. Scarfi, L.; Langer, H.; Messina, A.; Musumeci, C. Tectonic Regimes Inferred from Clustering of Focal Mechanisms and Their Distribution in Space: Application to the Central Mediterranean Area. *J. Geophys. Res. Solid Earth* **2021**, *126*, e2020JB020519. <https://doi.org/10.1029/2020jb020519>.
41. Alparone, S.; Barberi, G.; Bonforte, A.; Maiolino, V.; Ursino, A. Evidence of multiple strain fields beneath the eastern flank of Mt. Etna volcano (Sicily, Italy) deduced from seismic and geodetic data during 2003–2004. *Bull. Volcanol.* **2011**, *73*, 869–885. <https://doi.org/10.1007/s00445-011-0456-1>.
42. De Guidi, G.; Scudero, S.; Gresta, S. New insights into the local crust structure of Mt. Etna volcano from seismological and morphotectonic data. *J. Volcanol. Geotherm. Res.* **2012**, *223–224*, 83–92. <https://doi.org/10.1016/j.jvolgeores.2012.02.001>.
43. Bonaccorso, A.; Aloisi, M.; Mattia, M. Dike emplacement forerunning the Etna July 2001 eruption modeled through continuous tilt and GPS data. *Geophys. Res. Lett.* **2002**, *29*, 1–4. <https://doi.org/10.1029/2001gl014397>.
44. Bonanno, A.; Palano, M.; Privitera, E.; Gresta, S.; Puglisi, G. Magma intrusion mechanisms and redistribution of seismogenic stress at Mt. Etna volcano (1997–1998). *Terra Nova* **2011**, *23*, 339–348. <https://doi.org/10.1111/j.1365-3121.2011.01019.x>.
45. Bonforte, A.; Guglielmino, F.; Puglisi, G. Large dyke intrusion and small eruption: The December 24, 2018 Mt. Etna eruption imaged by Sentinel-1 data. *Terra Nova* **2019**, *31*, 405–412. <https://doi.org/10.1111/ter.12403>.
46. De Novellis, V.; Atzori, S.; De Luca, C.; Manzo, M.; Valerio, E.; Bonano, M.; Cardaci, C.; Castaldo, R.; Di Bucci, D.; Manunta, M.; et al. DInSAR Analysis and Analytical Modeling of Mount Etna Displacements: The December 2018 Volcano-Tectonic Crisis. *Geophys. Res. Lett.* **2019**, *46*, 5817–5827. <https://doi.org/10.1029/2019gl082467>.
47. Barreca, G.; Corradino, M.; Monaco, C.; Pepe, F. Active Tectonics along the South East Offshore Margin of Mt. Etna: New Insights from High-Resolution Seismic Profiles. *Geosciences* **2018**, *8*, 62. <https://doi.org/10.3390/geosciences8020062>.

48. Cocina, O.; Neri, G.; Privitera, E.; Spampinato, S. Stress tensor computations in the Mount Etna area (Southern Italy) and tectonic implications. *J. Geodyn.* **1997**, *23*, 109–127. [https://doi.org/10.1016/s0264-3707\(96\)00027-0](https://doi.org/10.1016/s0264-3707(96)00027-0).
49. Lanzafame, G.; Neri, M.; Coltelli, M.; Lodato, L.; Rust, D. North–South compression in the Mt. Etna region (Sicily): Spatial and temporal distribution. *Acta Vulcanol.* **1997**, *9*, 121–133.
50. Patanè, D.; Privitera, E. Seismicity related to 1989 and 1991–1993 Mt. Etna (Italy) eruptions: Kinematic constraints by FPS analysis. *J. Volcanol. Geother. Res.* **2001**, *109*, 77–98.
51. Labaume, P.; Bousquet, J.C.; Lanzafame, G. Early deformation at a submarine compressive front: The Quaternary Catania fore-deep south of Mt. Etna, Sicily, Italy. *Tectonophysics* **1990**, *177*, 349–366.
52. Ristuccia, G.M.; Di Stefano, A.; Gueli, A.M.; Monaco, C.; Stella, G.; Troja, S.O. OSL chronology of Quaternary terraced deposits outcropping between Mt. Etna volcano and the Catania Plain (Sicily, southern Italy). *Phys. Chem. Earth Parts* **2013**, *63*, 36–46. <https://doi.org/10.1016/j.pce.2013.03.002>.
53. Bonforte, A.; Guglielmino, F.; Coltelli, M.; Ferretti, A.; Puglisi, G. Structural assessment of Mount Etna volcano from Permanent Scatterers analysis. *Geochem. Geophys. Geosyst.* **2011**, *12*, 1–19. <https://doi.org/10.1029/2010gc003213>.
54. Gross, F.; Krastel, S.; Geersen, J.; Behrmann, J.H.; Ridente, D.; Chiocci, F.L.; Bialas, J.; Papenberg, C.; Cukur, D.; Urlaub, M.; et al. The limits of seaward spreading and slope instability at the continental margin offshore Mt Etna, imaged by high-resolution 2D seismic data. *Tectonophysics* **2016**, *667*, 63–76. <https://doi.org/10.1016/j.tecto.2015.11.011>.
55. Branca, S.; De Guidi, G.; Lanzafame, G.; Monaco, C. Holocene vertical deformation along the coastal sector of Mt. Etna volcano (eastern Sicily, Italy): Implications on the time–space constraints of the volcano lateral sliding. *J. Geodyn.* **2014**, *82*, 194–203. <https://doi.org/10.1016/j.jog.2014.07.006>.
56. Govers, R.; Wortel, M. Lithosphere tearing at STEP faults: Response to edges of subduction zones. *Earth Planet. Sci. Lett.* **2005**, *236*, 505–523. <https://doi.org/10.1016/j.epsl.2005.03.022>.
57. Gambino, S.; Barreca, G.; Gross, F.; Monaco, C.; Krastel, S.; Gutscher, M.-A. Deformation Pattern of the Northern Sector of the Malta Escarpment (Offshore SE Sicily, Italy): Fault Dimension, Slip Prediction, and Seismotectonic Implications. *Front. Earth Sci.* **2021**, *8*, 1–20. <https://doi.org/10.3389/feart.2020.594176>.
58. Musumeci, C.; Scarfi, L.; Palano, M.; Patanè, D. Foreland segmentation along an active convergent margin: New constraints in southeastern Sicily (Italy) from seismic and geodetic observations. *Tectonophysics* **2014**, *630*, 137–149. <https://doi.org/10.1016/j.tecto.2014.05.017>.
59. Chiocci, F.L.; Coltelli, M.; Bosman, A.; Cavallaro, D. Continental margin large-scale instability controlling the flank sliding of Etna volcano. *Earth Planet. Sci. Lett.* **2011**, *305*, 57–64. <https://doi.org/10.1016/j.epsl.2011.02.040>.
60. C.N.R. *Geological Map of Mt. Etna. Scale 1:50,000*; L.A.C.: Florence, Italy, 1979.
61. Mattia, M.; Bruno, V.; Montgomery-Brown, E.; Patanè, D.; Barberi, G.; Coltelli, M. Combined seismic and geodetic analysis before, during and after the 2018 Mt. Etna eruption. *Geochem. Geophys. Geosyst.* **2020**, *21*, e2020GC009218. <https://doi.org/10.1029/2020gc009218>.
62. Civico, R.; Pucci, S.; Nappi, R.; Azzaro, R.; Villani, F.; Pantosti, D.; Cintì, F.R.; Pizzimenti, L.; Branca, S.; Brunori, C.A.; et al. Surface ruptures following the 26 December 2018, Mw 4.9, Mt. Etna earthquake, Sicily (Italy). *J. Maps* **2019**, *15*, 831–837. <https://doi.org/10.1080/17445647.2019.1683476>.
63. Rasà, R.; Azzaro, R.; Leonardi, O. Aseismic Creep on Faults and Flank Instability at Mt. Etna Volcano, Sicily. In *Volcano Instability on the Earth and Other Planets*; McGuire, W.C., Jones, A.P., Neuberg, J., Eds.; Geological Society Special Publication; The Geological Society: London, UK, 1996; Volume 110, pp. 179–192.
64. Azzaro, R.; D’Amico, S.; Mostaccio, A.; Scarfi, L.; Tuvè, T. Terremoti con effetti macrosismici in Sicilia orientale nel periodo Gennaio 2002–Dicembre 2005. *Quad. Geof.* **2006**, *41*, 62.
65. De Guidi, G.; Brighenti, F.; Carnemolla, F.; Imposa, S.; Marchese, S.A.; Palano, M.; Scudero, S.; Vecchio, A. The unstable eastern flank of Mt. Etna volcano (Italy): First results of a GNSS-based network at its southeastern edge. *J. Volcanol. Geotherm. Res.* **2018**, *357*, 418–424. <https://doi.org/10.1016/j.jvolgeores.2018.04.027>.
66. Carlino, M.F.; Cavallaro, D.; Coltelli, M.; Cocchi, L.; Zgur, F.; Patanè, D. Time and space scattered volcanism of Mt. Etna driven by strike-slip tectonics. *Sci. Rep.* **2019**, *9*, 12125. <https://doi.org/10.1038/s41598-019-48550-1>.
67. Bruno, V.; Mattia, M.; Aloisi, M.; Palano, M.; Cannavò, F.; Holt, W.E. Ground deformations and volcanic processes as imaged by CGPS data at Mt. Etna (Italy) between 2003 and 2008. *J. Geophys. Res. Earth Surf.* **2012**, *117*, 1–23. <https://doi.org/10.1029/2011jb009114>.
68. Aloisi, M.; Mattia, M.; Ferlito, C.; Palano, M.; Bruno, V.; Cannavò, F. Imaging the multi-level magma reservoir at Mt. Etna volcano (Italy). *Geophys. Res. Lett.* **2011**, *38*, L16306. <https://doi.org/10.1029/2011gl048488>.
69. Bruno, V.; Mattia, M.; Montgomery-Brown, E.; Rossi, M.; Scandura, D. Inflation Leading to a Slow Slip Event and Volcanic Unrest at Mount Etna in 2016: Insights from CGPS Data. *Geophys. Res. Lett.* **2017**, *44*, 12–141. <https://doi.org/10.1002/2017gl075744>.
70. Herring, T.A.; Floyd, M.A.; King, R.W.; McClusky, S.C. GLOBK: Global Kalman Filter VLBI and GPS Analysis Program. In *Reference Manual*; Massachusetts Institute of Technology: Cambridge, UK, 2015.
71. Herring, T.A.; King, R.W.; Floyd, M.A.; McClusky, S.C. GPS Analysis at MIT. In *GAMIT Reference Manual*; Massachusetts Institute of Technology: Cambridge, UK, 2018.
72. Haines, A.J.; Holt, W.E. A procedure for obtaining the complete horizontal motions within zones of distributed deformation from the inversion of strain rate data. *J. Geophys. Res. Earth Surf.* **1993**, *98*, 12057–12082. <https://doi.org/10.1029/93jb00892>.

73. Holt, W.E.; Haines, A.J. The kinematics of northern South Island, New Zealand, determined from geologic strain rates. *J. Geophys. Res. Earth Surf.* **1995**, *100*, 17991–18010. <https://doi.org/10.1029/95jb01059>.
74. Haines, A.J.; Jackson, A.; Holt, W.E.; Agnew, D.C. *Representing Distributed Deformation by Continuous Velocity Fields*; Science Report 1998, 98/5; Institute of Geology and Nuclear Science: Wellington, New Zealand, 1998.
75. Krastel, S. Short cruise report: MAGOMET—Offshore Flank Movement of Mount Etna and Associated Landslide Hazard in the Ionian Sea (Mediterranean Sea). In Proceedings of the RV Poseidon-Cruise POS496, Malaga, Catania, 24 March–4 April 2016; Christian-Albrechts-Universität zu Kiel, Institute of Geosciences: Kiel, Germany, 2016; 8p.
76. Gutscher, M.-A.; Kopp, H.; Krastel, S.; Bohrmann, G.; Garlan, T.; Zaragosi, S.; Klauke, I.; Wintersteller, P.; Loubrieu, B.; Le Faou, Y.; et al. Active tectonics of the Calabrian subduction revealed by new multi-beam bathymetric data and high-resolution seismic profiles in the Ionian Sea (Central Mediterranean). *Earth Planet. Sci. Lett.* **2017**, *461*, 61–72. <https://doi.org/10.1016/j.epsl.2016.12.020>.
77. Camerlenghi, A.; Del Ben, A.; Hübscher, C.; Forlin, E.; Geletti, R.; Brancatelli, G.; Micallef, A.; Saule, M.; Facchin, L. Seismic markers of the Messinian salinity crisis in the deep Ionian Basin. *Basin Res.* **2020**, *32*, 716–738. <https://doi.org/10.1111/bre.12392>.
78. Micallef, A.; Camerlenghi, A.; Garcia-Castellanos, D.; Otero, D.C.; Gutscher, M.-A.; Barreca, G.; Spatola, D.; Facchin, L.; Geletti, R.; Krastel, S.; et al. Evidence of the Zanclean megaflood in the eastern Mediterranean Basin. *Sci. Rep.* **2018**, *8*, 1078. <https://doi.org/10.1038/s41598-018-19446-3>.
79. Gaillot, A.; Gutscher, M.A.; Murphy, S.; Klingelhoefer, F. Micro-Bathymetric Mapping of the North Alfeo Strike-Slip Fault (Off-shore Catania Sicily): Preliminary Results from the FocusX1 Expedition. In Proceedings of the EGU General Assembly 2021, Online, 19–30 April 2021; EGU21-2731. <https://doi.org/10.5194/egusphere-egu21-2731>.
80. Scandone, P.; Patacca, E.; Radoicic, R.; Ryan, W.B.F.; Cita, M.B.; Rawson, M.; et al. Mesozoic and Cenozoic rocks from Malta escarpment (Central Mediterranean). *AAPG Bull.* **1981**, *65*, 1299–1319.
81. Catalano, R.; Franchino, A.; Merlini, S.; Sulli, A. A crustal section on the eastern Algerian basin to the Ionian ocean (central Mediterranean). *Mem. Soc. Geol. It.* **2000**, *55*, 71–85.
82. Barreca, G. Geological and geophysical evidences for mud diapirism in south-eastern Sicily (Italy) and geodynamic implications. *J. Geodyn.* **2014**, *82*, 168–177. <https://doi.org/10.1016/j.jog.2014.02.003>.
83. Polonia, A.; Torelli, L.; Gasperini, L.; Cocchi, L.; Muccini, F.; Bonatti, E.; Hensen, C.; Schmidt, M.; Romano, S.; Artoni, A.; et al. Lower plate serpentinite diapirism in the Calabrian Arc subduction complex. *Nat. Commun.* **2017**, *8*, 1–13. <https://doi.org/10.1038/s41467-017-02273-x>.
84. Woodcock, N.H.; Fischer, M. Strike-slip duplexes. *J. Struct. Geol.* **1986**, *8*, 725–735. [https://doi.org/10.1016/0191-8141\(86\)90021-0](https://doi.org/10.1016/0191-8141(86)90021-0).
85. Amato, A.; Azzara, R.; Basili, A.; Chiarabba, C.; Cocco, M.; Di Bona, M.; Selvaggi, G. Decembr 13, 1990 Eastern Sicily earthquake. *Ann. Geofis.* **1995**, *38*, 255–266.
86. Zhang, H.; Thurber, C.; Bedrosian, P. Joint inversion for Vp, Vs, and Vp/Vs at SAFOD, Parkfield, California. *Geochem. Geophys. Geosystems* **2009**, *10*, Q11002. <https://doi.org/10.1029/2009gc002709>.
87. De Guidi, G.; Caputo, R.; Scudero, S. Regional and local stress field orientation inferred from quantitative analyses of extension joints: Case study from southern Italy. *Tectonics* **2013**, *32*, 239–251.
88. Fossen, H. *Structural Geology*, 2nd ed.; Cambridge University Press: Cambridge, UK, 2016; 524p. ISBN 9781107057647.
89. Woodcock, N.H.; Schubert, C. Continental Strike-Slip Tectonics. In *Continental Deformation*; Hancock, P.L., Ed.; Pergamon Press: New York, NY, USA, 1994; pp. 251–263.
90. Sylvester, A.G. Strike-slip faults. *Geol. Soc. of Am. Bull.* **1988**, *100*, 1666–1703.
91. Spampinato, C.R.; Scicchitano, G.; Ferranti, L.; Monaco, C. Raised Holocene paleo-shorelines along the Capo Schisò coast, Taormina: New evidence of recent co-seismic deformation in northeastern Sicily (Italy). *J. Geodyn.* **2012**, *55*, 18–31. <https://doi.org/10.1016/j.jog.2011.11.007>.
92. Murru, M.; Montuori, C.; Wyss, M.; Privitera, E. The locations of magma chambers at Mt. Etna, Italy, mapped by-values. *Geophys. Res. Lett.* **1999**, *26*, 2553–2556. <https://doi.org/10.1029/1999gl900568>.
93. Patanè, D.; Chiarabba, C.; De Gori, P.; Bonaccorso, A. Magma ascent and the pressurization of Mt. Etna’s volcanic system. *Science* **2003**, *299*, 2061–2063.
94. Patanè, D.; Mattia, M.; Aloisi, M. Shallow intrusive processes during 2002–2004 and current volcanic activity on Mt. Etna. *Geophys. Res. Lett.* **2005**, *32*, L06302. <https://doi.org/10.1029/2004gl021773>.
95. Patanè, D.; Barberi, G.; Cocina, O.; De Gori, P.; Chiarabba, C. Time-Resolved Seismic Tomography Detects Magma Intrusions at Mount Etna. *Science* **2006**, *313*, 821–823. <https://doi.org/10.1126/science.1127724>.
96. De Gori, P.; Chiarabba, C.; Patanè, D. Qpstructure of Mount Etna: Constraints for the physics of the plumbing system. *J. Geophys. Res. Earth Surf.* **2005**, *110*, B05303. <https://doi.org/10.1029/2003jb002875>.
97. Mazzarini, F.; Armienti, P. Flank Cones at Mount Etna Volcano: Do they have a power-law distribution? *Bull. Volcanol.* **2001**, *62*, 420–430. <https://doi.org/10.1007/s004450000109>.
98. Favalli, M.; Karátson, D.; Mazzarini, F.; Pareschi, M.T.; Boschi, E. Morphometry of scoria cones located on a volcano flank: A case study from Mt. Etna (Italy), based on high-resolution LiDAR data. *J. Volcanol. Geotherm. Res.* **2009**, *186*, 320–330. <https://doi.org/10.1016/j.jvolgeores.2009.07.011>.
99. Ferlito, C. Mount Etna volcano (Italy). Just a giant hot spring!. *Earth-Sci. Rev.* **2018**, *177*, 14–23. <https://doi.org/10.1016/j.earscirev.2017.10.004>.

100. Ferlito, C.; Viccaro, M.; Cristofolini, R. Volatile-rich magma injection into the feeding system during the 2001 eruption of Mt. Etna (Italy): Its role on explosive activity and change in rheology of lavas. *Bull. Volcanol.* **2009**, *71*, 1149–1158. <https://doi.org/10.1007/s00445-009-0290-x>.
101. Ferlito, C.; Coltorti, M.; Lanzafame, G.; Giacomoni, P.P. The volatile flushing triggers eruptions at open conduit volcanoes: Evidence from Mount Etna volcano (Italy). *Lithos* **2014**, *184–187*, 447–455. <https://doi.org/10.1016/j.lithos.2013.10.030>.
102. Uslular, G.; Le Corvec, N.; Mazzarini, F.; Legrand, D.; Gençlioğlu-Kuşcu, G. Morphological and multivariate statistical analysis of quaternary monogenetic vents in the Central Anatolian Volcanic Province (Turkey): Implications for the volcano-tectonic evolution. *J. Volcanol. Geotherm. Res.* **2021**, *416*, 107280. <https://doi.org/10.1016/j.jvolgeores.2021.107280>.
103. Mazzuoli, R.; Tortorici, L.; Ventura, G. Oblique rifting in Salina, Lipari and Vulcano islands (Aeolian islands, southern Italy). *Terra Nova* **1995**, *7*, 444–452. <https://doi.org/10.1111/j.1365-3121.1995.tb00540.x>.
104. Vries, B.V.W.D.; Merle, O. Extension induced by volcanic loading in regional strike-slip zones. *Geology* **1998**, *26*, 983–986. [https://doi.org/10.1130/0091-7613\(1998\)0262.3.co;2](https://doi.org/10.1130/0091-7613(1998)0262.3.co;2).
105. Alaniz-Álvarez, S.; Nieto-Samaniego, A.; Morán-Zenteno, D.; Aldave, L.A.A. Rhyolitic volcanism in extension zone associated with strike-slip tectonics in the Taxco region, southern Mexico. *J. Volcanol. Geotherm. Res.* **2002**, *118*, 1–14. [https://doi.org/10.1016/s0377-0273\(02\)00247-0](https://doi.org/10.1016/s0377-0273(02)00247-0).
106. Di Giuseppe, P.; Agostini, S.; Lustrino, M.; Karaoğlu, Ö.; Savaşçın, M.Y.; Manetti, P.; Ersoy, Y. Transition from Compression to Strike-slip Tectonics Revealed by Miocene–Pleistocene Volcanism West of the Karlıova Triple Junction (East Anatolia). *J. Pet.* **2017**, *58*, 2055–2087. <https://doi.org/10.1093/petrology/egx082>.